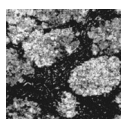# Architecture, paleosols and cyclicity of the Middle–Late Pennsylvanian proximal fluvial system (Nýřany Member, Pilsen Basin, Czech Republic)

RICHARD LOJKA, NICHOLAS A. ROSENAU, TAMARA SIDORINOVÁ & LADISLAV STRNAD

The Nýřany Member in the Pilsen Basin records the evolution of a broad paleotropical alluvial plain that preserves amalgamated lenticular to sheet sandstone bodies separated by basin-wide floodplains. Facies and architectural element analysis in conjunction with well-log correlation was employed in order to reconstruct fluvial system stacking patterns and decipher the controls responsible for the preserved fluvial architectures and identify the possible influence of allogenic processes on basin fill architectures. The main architectural components identified include: 1) sheet-like and lenticular pebbly to cobbly conglomerate thalweg fill representing the lowermost portion of channels that are preferentially preserved; 2) inclined gravel-sand and sandy strata of barforms and rarely preserved (3) mudstone units representing floodplains and abandoned channel fills. These architectural elements combine to form a hierarchy of alluvial cycles represented by channel-bar systems (3–10 m thick), channel-belts (4–15 m thick) and stacked channel-belt complexes (10–35 m thick). Autogenic processes of lateral migration and local and regional avulsion of braided channels of intermediate sinuosity (1.5) controlled the formation of the smaller scale cycles. While the geometry of stacked channel belt complexes (sandbodies) appear to be driven by variations in subsidence rates, their cyclic alternation with extensive floodplains is considered to be related to allogenic processes of variable seasonality of precipitation, which affected sedimentation rates and water-table level in the basin. Their maximum periodicity of 140 k.y. indicate that eccentricity paced changes of Earth's orbit may be a driving force controlling climate stability in the Pennsylvanian paleotropics. • Key words: alluvial cycles, perennial braided streams, Vertisol, tree trunk silicification, Pennsylvanian.

Richard Lojka (corresponding author) & Tamara Sidorinová, Czech Geological Survey, Klárov 3/131, 118 21 Praha 1, Czech Republic; richard.lojka@geology.cz • Nicholas A. Rosenau, Southern Methodist University, Huffington Department of Earth Sciences, 3225 Daniel Ave., Dallas, TX, USA, current address: Pioneer Natural Resources, 5205 N O'Connor Blvd., Suite 200, 75039 Irving, TX, USA • Ladislav Strnad, Charles University, Faculty of Sciences, Albertov 6, 128 43 Praha 2, Czech Republic

The architecture of a tropical gravel-bed dominated fluvial system of Asturian–Cantabrian age in the Pilsen Basin preserves a hierarchy of cycles that range from metres to decametres in thickness and display systematic fining upward grain sizes from amalgamated cobble conglomerate and pebbly sandstone with numerous erosional surfaces to mudstone bearing paleosols and coal seams. While the small-scale alluvial cycles have commonly been attributed to autogenic processes such as local and regional avulsions, the origin of large-scale decametres thick cycles is less clear and has been interpreted to reflect base-level (*i.e.*, sea-level) rises and falls (*e.g.*, Allen 1983, Godin 1991, Wright & Marriott 1993, Shanley & McCabe 1994, Atchley *et al.* 2004). This interpretation is supported by

evidence of brackish or marine water incursions during periods of mudstone-dominated deposition in other basins (Allen & Fielding 2007, McLaurin & Steel 2007). Similar decametres thick alluvial cycles, however, are also observed in hinterland basins far from marine influence and filled solely by continental strata. The origin and architecture of these large-scale alluvial cycles in continental setting remain uncertain.

The investigated fluvial system of the Nýřany Member preserves a 2 m.y. interval of alluvial deposition across the Moscovian–Kasimovian (Westphalian–Stephanian) transition, which is characterized by the collapse of Euroamerican coal forests and the expansion of red beds (*e.g.*, DiMichele *et al.* 2001). Aridification recorded in paleosols

at southern high latitudes on Gondwana suggests a global change of climate towards warmer and dryer conditions across the Moscovian–Kasimovian (Gulbranson *et al.* 2015). The contraction of coal-forests is proposed to have increased atmospheric CO_2 levels leading to high latitude Gondwana deglaciation that further intensified the seasonality of precipitation in the Pangaean paleotropics (*e.g.*, Cleal *et al.* 1999, Cleal & Thomas 2005, Schneider *et al.* 2006, Tabor & Poulsen 2008, Allen *et al.* 2011). Additionally, there is strong evidence in coastal basins for numerous high-frequency (10^4–10^5 years) sea-level changes during the Middle–Late Pennsylvanian suggesting persistent ice volume fluctuations (*e.g.*, Gibling & Bird 1994, Feldman *et al.* 2005, Rygel *et al.* 2008, Birgenheier *et al.* 2009).

The present study seeks to decipher cyclic patterns within the Nýřany Member fluvial system and identify their possible controls and potential response of fluvial system to changing environment across the Westphalian–Stephanian transition in the central-east Pangaean paleotropics (Fig. 1A). Structure, mineralogy, and geochemistry of intercalated paleosols allow for precise quantitative paleoprecipitation estimates of the equatorial Middle–Late Pennsylvanian climate.

Geological setting

Central and Western Bohemian basins

The Central and Western Bohemian basins (CWB) compose the largest intramontane basin in the Bohemian Massif formed during early post-orogenic extension associated with strike-slip and wrench faulting (Havlena & Pešek 1980, Pašek & Urban 1990, Pešek 1994, Pešek *et al.* 1998). The NE–SW oriented basin is consistent with the prominent tectonic boundary between Teplá-Barrandian and Saxo-Thuringian terranes situated close to the faulted north-western basin margin (Fig. 1B). Deposition initiated in several small depocentres that gradually expanded to a single large depocentre (*ca* 6500 km^2) during the early Stephanian (Havlena 1977). Uplift and denudation led to a complex of larger basins (*e.g.*, Pilsen Basin, Fig. 1C) surrounded by small erosional relics that share common lithostratigraphic packages. However, the thickness and lithofacies distribution of stratigraphic units vary between basins reflecting spatial differences in accommodation, sediment supply and subsidence (*e.g.*, Havlena & Pešek 1980). Up to 1500 m of terrestrial sediments were deposited from the Middle Pennsylvanian (Moscovian) to Cisuralian (Asselian) and are divided into the Kladno, Týnec, Slaný and Líně formations (Fig. 1D) based upon lithology and floral communities (*e.g.*, Weithofer 1896, Havlena & Pešek 1980, Pešek 1994). The lower part of the basin fill is dominated by fluvial to alluvial plain deposits of the Kladno and

Týnec formations, while the upper part of the basin fill consists mainly of lacustrine to alluvial plain facies represented by the Slaný and Líně formations. Synsedimentary tectonic activity was responsible for the gradual expansion of the depositional area, at least two basin-wide regional hiatuses, and a prominent change from fluvial-dominated environments to lacustrine-dominated environments in the early Gzhelian (Skoček 1968, 1990; Havlena & Pešek 1980; Pešek 1994).

During the Middle to Late Pennsylvanian, the CWB was situated close to the centre of the Variscan Mountains (Fig. 1A), about 400 km south of the North Variscan Foreland Basin and probably less than 500 km north of the Paleotethys Ocean (Scotese & McKerrow 1990, Ziegler 1990). Paleomagnetic data indicate a paleolatitude about 4° to 6° N (Krs & Pruner 1995). Central Bohemia was drained north-westward and later also north-eastward to the North Variscan Foreland Basin via the Saxonian and Lausatian basins, respectively. Western Bohemia, including the Pilsen Basin, was at least initially most likely drained south-westward to the Naab Basin in Bavaria (Opluštil 2005). A minimal paleoelevation of a few hundred metres has been estimated for the Pilsen Basin based on (1) the presumed length and gradient of the drainage system, (2) absence of marine or brackish incursions, and (3) the similarity of paleoflora communities between the Pilsen Basin and those of coeval paralic basins (Opluštil 2005, Bashforth *et al.* 2011).

Pilsen Basin

The Pilsen Basin is located at the south-western part of the CWB and covers an area of approximately 550 km^2 (Fig. 1C). It forms a 40 km long and approximately 15 km wide NNE–SSW oriented graben structure that is filled by more than 850 m of late Paleozoic terrestrial strata. The area of maximum thickness is concentrated along a narrow (*ca* 3 km) trench in the basin center (Pešek 1968, Pašek & Urban 1990), which continues northward forming the 20 km long and narrow (*ca* 5 km wide) graben structure of the Žihle Basin (Elznic *et al.* 1974). The central trench of the Pilsen Basin formed in response to N–S compression accompanied by dextral strike-slip faulting on oblique NW–SE oriented faults and normal faulting on N–S conjugate faults (Pašek & Urban 1990). Starting with the Nýřany Member, the tectonic compression shifted slightly to the NNW–SSE resulting in amplification of normal faulting on NW–SE faults. Active fault tectonics controlled the axial drainage and sediment supply from north-west to north as indicated by the relative sand and gravel proportions (Pešek 1968, 1994).

The Pilsen Basin preserves evidence of a relatively shallow burial history and low paleotemperatures, in con-
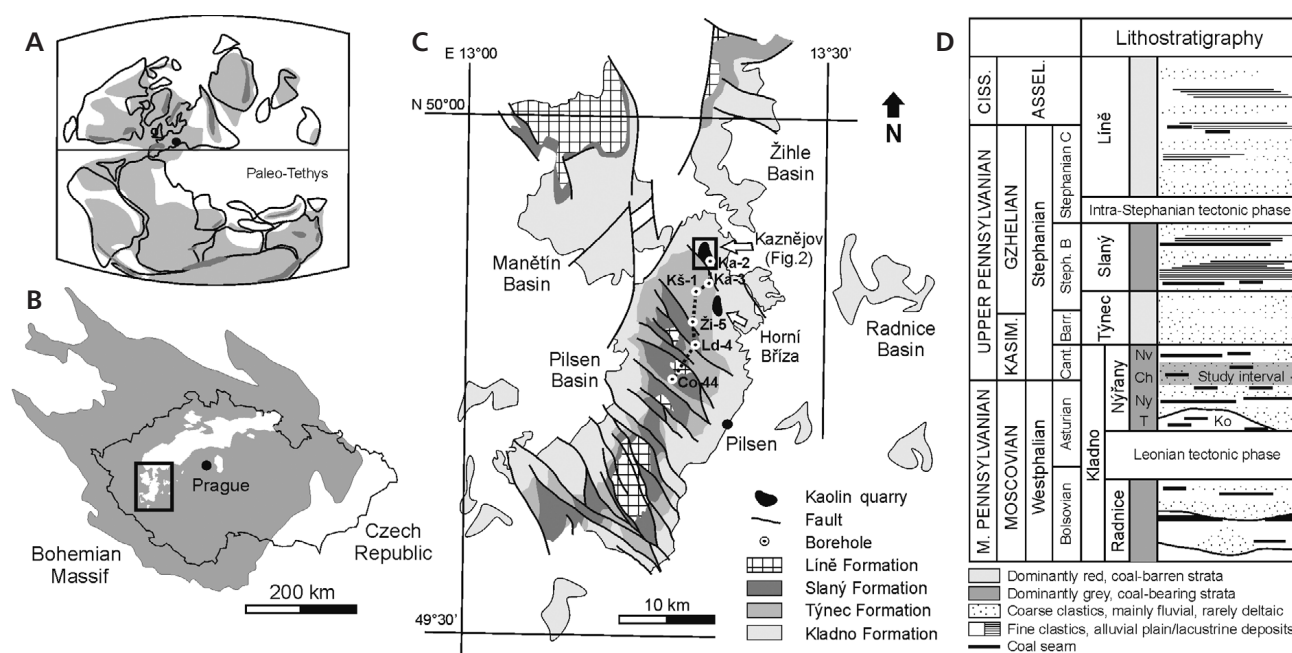
Figure 1. Location of the study area. • A – Middle–Late Pennsylvanian paleogeography showing position of the Bohemian Massif near the paleoequator in central-east Pangaea. • B – late Paleozoic continental basins in western, central and north-eastern Czech Republic arranged along the prominent NE-trending tectonic boundary of the Teplá-Barrandian and Saxo-Thuringian terranes. • C – close-up of Western Bohemian basins and surrounding relics, position of the two studied kaolin quarries in the northern part of the Pilsen Basin and location of cross-section in Fig. 10 are indicated. Deposits of the Kladno and Týnec formations are grouped together in the Manětín and Žihle basins. • D – simplified stratigraphy of the Western and Central Bohemian Basin. Stage boundaries are modified after Opluštil *et al.* (2016). Nýřany Member stratigraphic units: Ko – Komberk Horizon, T – Touškov group of seams, Ny – Nýřany group of seams, Ch – Chotíkov group of seams, Nv – Nevřeň group of seams.

trast to central and north-eastern Bohemia (Pešek *et al.* 2001, Lojka *et al.* 2010). Vitrinite reflectance (R_o) values of the Nýřany Member coal seams vary between 0.5–0.58% in the study area (Kš-1 well, Fig. 1C).

Nýřany Member

The Nýřany Member represents the upper unit of the Kladno Formation (Fig. 1D) and reaches a maximum thickness of about 350 m in the Pilsen Basin. It unconformably overlies the Radnice Member representing the basal part of the basin fill, which is confined to a central trench of the Pilsen Basin and oblique bedrock-incised paleovalleys, where up to 10 m thick coal seams formed apart from the axial drainage (Havlena & Pešek 1980, Pešek 1994). The basal surface of the Nýřany Member corresponds to a prominent regional erosional surface that reflects the expansion of the depositional area to the N, NW and SW and represents a time period sufficiently long to disrupt the continuity of flora (Němejc 1953).

Strata of the Nýřany Member accumulated on a broad alluvial plain that blanketed an incompletely peneplained plateau punctuated by low ridges of emergent Neoproterozoic and lower Paleozoic basement rocks (Havlena & Pešek 1980, Pešek 1994, Pešek *et al.* 1998, Bashforth *et* *al.* 2011). The depositional settings of the Nýřany Member alluvial plain are not well constrained due to limited exposures that are typically restricted to small and scattered outcrops. Opluštil & Pešek (1998) and Pešek *et al.* (1998) proposed a rough regional subdivision of the Nýřany Member into four lithological units based on the proportion of "coarse" (medium- to very coarse-grained sandstone and conglomerate) versus "fine" strata observed in > 1000 borehole cores across the CWB. The proposed lithological units reflect a suite of depositional environments varying from "proximal braided-river plain/alluvial fan, distal braided-river plain, anastomosing/meandering-river plain to lacustrine/wetland". Following this subdivision, the area of the Pilsen Basin corresponds to a distal braided-river plain depositional environment characterized by a dominance of "coarse" strata with subordinate fine-grained intercalations bearing laterally discontinuous coal seams.

In the Pilsen Basin, the Nýřany Member coal seams are grouped into four stratigraphic levels (Fig. 1D) based upon their stratigraphic position, floral assemblage and palynospectra (Šetlík 1968, 1977, 1980; Pešek 1994). The lowermost Touškov group of coal seams is locally developed close to the base of the Nýřany Member and contains up to four coal seams, the thickest of which is 3 m. Coal seams are intercalated with laminated lacustrine deposits
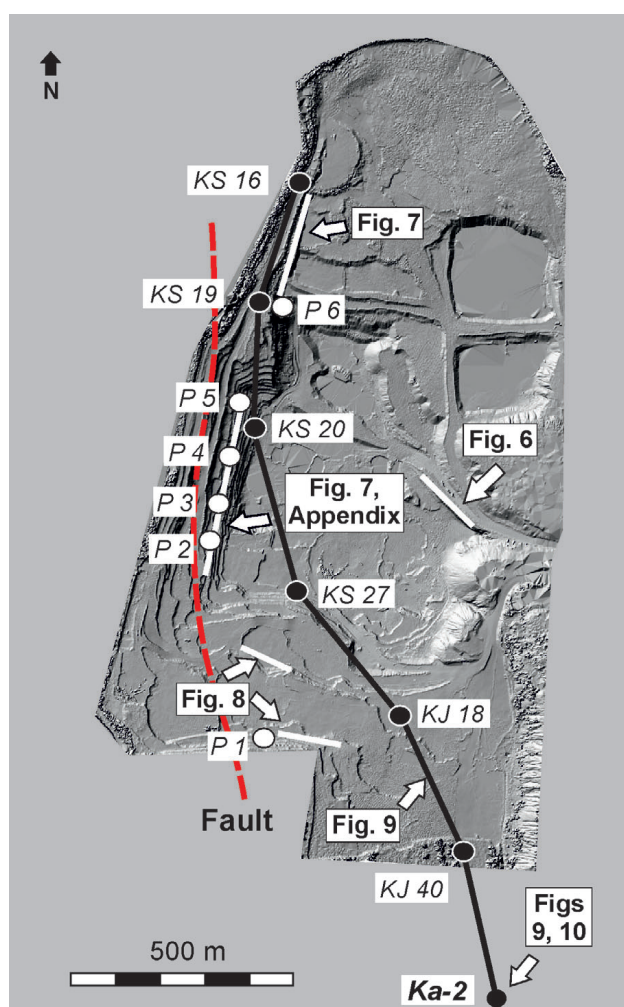
Figure 2. Digital elevation model of the Kaznějov quarry showing position of photopanels (white lines), measured sections (white dots) and well-logs (black dots) including location of cross section (black line) depicted in Fig. 9.

and grey to variageted paleosols that form about 50 m thick unit of dominantly fine-grained strata of the so-called Komberk horizon (Pešek 1968). Floral assemblages indicate a late Westphalian (Asturian) age for this unit as well as that of the overlying Nýřany group of coal seams, which comprises up to three laterally extensive coal seams. Beginning in the middle part of the Nýřany Member there is a gradational shift in palynospectra towards a diversification of ferns recorded in the Chotíkov group of coal seams that spans a thick stratigraphic interval (*ca* 150 m) and composes five up to 1.5 m thick coal seams, within which early Stephanian (Cantabrian) plant community appears. The uppermost Nevřeň group of seams is developed at the northern part of the Pilsen Basin on top of the Nýřany Member and is composed of two coal seams containing early Stephanian (Cantabrian) flora. It is associated with a volcanic ash layer that is

dated to 305.99 ± 0.07 Ma, while the volcanic ash layer from the lowermost Touškov group of coal seams is dated to 308.00 ± 0.04 Ma resulting in an at least two million year long interval of Nýřany Member deposition (Opluštil *et al.* 2016).

The precise stratigraphic position of the studied section in the northern part of the Pilsen Basin exposed in the two kaolin quarries (Fig. 1C) remains obscure particularly because of the absence of fossiliferous mudstones and similarity to overlying deposits of the Týnec Formation. It is developed, however, about 200–250 m above the Proterozoic basement, which is the stratigraphic level corresponding to the Chotíkov coal seams of the lowermost Stephanian (Cantabrian) age.

Methods

Field

The Kaznějov quarry is situated near the present day basin margin, 2.5 km north of the Horní Bříza quarry which is located basin-ward (Fig. 1C). The Kaznějov kaolin quarry exposes approximately 80 m thick fluvial succession over an area of 1400 × 700 m and provides extensive outcrops up to 50 m high. In contrast, the Horní Bříza kaolin quarry exposes about 40 m of fluvial strata over an area of approximately 800 × 400 m providing smaller outcrops rendering it less suitable for architectural analysis of large-scale fluvial features. Sedimentary facies and architectures are observed at both locations; however, detailed architectural analysis was primarily carried out at the Kaznějov quarry due to better exposure of the fluvial strata. Six stratigraphic sections with a cumulative thickness exceeding 130 m were measured in order to identify sedimentary facies. Sedimentary facies were defined based upon their structures, grain sizes and geometries. Fluvial facies coding broadly follows the scheme proposed by Miall (1996). Paleocurrent directions were measured using trough cross-strata and axes of trough-cross bedding. Accretion directions were measured on cross-bed and bedset bounding surfaces. Collectively, more than 200 measurements were taken throughout the studied sections. Photomosaics of outcrops were constructed in order to determine basic architectural elements and establish a hierarchy of bounding surfaces. Tens of structural boreholes and their lithological and gamma ray logs were studied in an effort to correlate the Nýřany Member in the northern part of the Pilsen basin. In order to correlate the prominent outcrop observations to structural boreholes additional historical core descriptions from exploration wells (ČGS – Geofond archive) located in the quarry area and nearby were studied. Paleosols were described and traced out in the field.

Laboratory

Thin-sections of paleosol matrix were studied and documented by a polarizing microscope (Nikon Eclipse 80i). Clay mineral fractions (< 2 μm) from each horizon were extracted following the conventional gravity settling method (Tanner & Jackson 1948). Oriented specimens for X-ray diffraction were prepared by the pipette method. Approximately 2 ml of suspension was dropped by pipette on the sample holder and air dried. The oriented specimens were analyzed air-dried and after 10 hours of saturation in ethylene glycol vapor at 60° C. The diffraction data were acquired on a Philips X´ Pert diffractometer using Cu$K\alpha$ radiation and a graphite secondary monochromator. The patterns of oriented specimens were collected in the angular range 2–50° 2Θ with steps of 0.05° 2Θ at 3 seconds per step. Clay mineral identification was performed using the NEWMOD code (Reynolds 1985). The major elements were determined using total digestion with mineral acids (HF-HCLO$_4$) and/or sintering (Na$_2$CO$_3$-NaNO$_3$) of samples (both in Pt dishes and/or crucibles) and subsequent chemical analysis. Al$_2$O$_3$, Fe$_2$O$_3$, MnO, MgO, CaO, Na$_2$O, K$_2$O P$_2$O$_5$ and TiO$_2$ were determined by ICP-OES. FeO was determined by potentiometric titration. SiO$_2$ and LOI (loss on ignition) were determined gravimetrically (Johnson & Maxwell 1981, Potts 1995).

Heavy mineral assemblages of coarse-grained sandstones (n = 11) were analysed in order to determine the provenance of the fluvial deposits. Two kilograms of each sandstone sample were disaggregated, washed in water to dissolve soluble salts and free the grains from adhering clays and iron oxide coatings. The samples were then dried and passed through a 0.5 mm mesh sieve. Afterwards, 50 g of each sample were separated using a high-density liquid (1,1,2,2-tetrabromoethane; d = 2.96). The heavy and light fractions were separated by gravity settling. The heavy fraction of each sample was subsequently investigated with a stereomicroscope (Nikon SMZ800) and polarizing microscope (Nikon Eclipse E600). A temporary grain mount for microscopic identification was implemented. The immersion liquid f. Merck, n = 1.516 was used. The magnetic minerals were detected by a permanent magnet. The semi-quantitative content of particular minerals, including opaque and secondary minerals, was calculated as a percentage volume in each sample.

Results and interpretations

Lithofacies and architectural components

Nine sedimentary lithofacies and subfacies are recognized in the exposures in both kaolin quarries (Table 1, Fig. 3). The lithofacies compose three major architectural components that differ in facies distribution and geometry. Measured sections with vertical facies trends are shown in Fig. 5. Photopanels and bedding diagrams of the Kaznějov quarry outcrops showing the stacking patterns of architectural components are presented in Figs 6–8 and online Appendix.

Erosionally based, sheet and lenticular conglomerate units

Description. – These dominantly cobbly to pebbly conglomerate units comprise sheets and lenses of the Gm, Gp and Gt facies that overlie planar, undulating or concave-up erosional surfaces and grade upwards to inclined gravel-sand and sandy strata. Their thicknesses range from single-cobble thick beds to 4.3 m thick composite conglomerate units that form extensive sheets (> 1000 m) in sections parallel to oblique to paleoflow, and lenticular bodies (< 100 m) in sections aproximately normal to paleoflow. Composite units contain clusters of planar and scoured erosional surfaces separating component beds (Fig. 3C). Large mudstone rip-up clasts occur commonly along these erosional surfaces typically in the Gm and Gp facies (Fig. 3A). When traced laterally, composite units tend to split into a suite of thin sheets (mainly Gm facies) that encompass several inclined gravel-sand and sandy strata.

Cobble-size conglomerate of the Gm facies forms sheets that overlie erosional surfaces and may thin laterally to single-cobble thick beds. These sheets are usually free of sandy matrix, display weak imbrication and contain mudstone rip-up clasts. The planar cross-bedded conglomerate of the Gp facies tends to overlie sheets of the Gm facies and fill scours. It forms simple large-scale inclined strata with variable angles of inclination (5–20°) that are typically composed of decimetre thick gravel-sand couplets (Fig. 3B). Medium-scale planar cross-beds usually consist of alternating openwork and bimodal gravel cross-laminae and stack laterally to form sheet-like bodies. Cross-beds of the Gt facies with pebbly sandstone interbeds (St$_g$ facies) may dominate in conglomerate units and form lenicular, gently inclined strata (Fig. 3C). Simple large-scale troughs of the Gt facies also occur. Rarely, composite conglomerate units encompass thin (< 0.2 m) and discontinuous (< 20 m) mudstone interbeds (Fig. 3H) as well as intraformational breccias of mudstone rip-up clasts accumulated along erosional concave-up and planar surfaces. Cobbles are dominated by quartz, quartz sandstone and chert. Weathered acid volcanics, quartz cemented lithic breccias and silicified tree trunks are locally observed (Fig. 4).

Interpretation. – The coarse nature of component facies, the number of erosional surfaces and common large mudstone rip-up clasts strongly suggest bedload deposition

from unidirectional traction currents in the thalweg or deepest portion of a channel. The highest energy flow conditions of maximum bankfull discharge were characterised by a flow velocity ranging from 5 to 8 m/s that is required to move gravel ranging in size from 20 to 30 cm at a depth of 1–10 m (Gustavson 1978). Cobble size conglomerates of the Gm facies represent amalgamated bedload sheets that formed diffuse longitudinal low-amplitude bed waves or transverse ribs that may have served as a capture of transporting material forming the channel bar nucleus (Ferguson 1993). Thin sheets of cobble conglomerate represent channel lags and pavements (Nemec & Postma 1993). Medium-scale planar cross-beds of the Gp facies represent accretionary bedforms of straight-crested dunes associated with bar deposits (Lunt *et al.* 2004). Low-angle inclined gravel-sand couplets probably represent the lower portions of lateral accretion surfaces on braid bars (Yagishita 1997). High-angle large-scale inclined bedsets may represent avalanche surfaces of lobate unit bars and scour fills or delta lobes of confluence bars (Bridge 1993b, Miall 1996, Yagishita 1997). Thalweg fills dominantly display downstream accretion with local indications of lateral accretion.

Medium-scale trough cross-beds of the Gt facies are interpreted to have been deposited from downstream migrating curved-crested dunes under high-energy conditions in deeper portions of the channel (Ramos & Sopena 1983, Bridge 1993b, Miall 1996). They may also be deposited on the lower parts of gently inclined accretionary bar surfaces (Gustavson 1978). It has been suggested that the preservation of gravel dunes requires a rapid recession of flow subsequent to a short duration of peak discharge (Khadkikar 1999). The prevalence of gravel dunes in the stratigraphic record would imply seasonal discharge fluctuations. Simple large-scale troughs may represent scour or pool fills associated with channel confluence zones (Ashmore 1993). Accumulations of large mudstone rip-up clasts along erosional surfaces most likely represent collapsed cut-banks and reworked abandoned channel fills deposited along incision surfaces.

Inclined gravel-sand and sandy strata

Description. – This architectural component is a single, large-scale (up to 6 m thick), gravel-sand or sandy inclined bedded unit. It is commonly gradational from the coarser, underlying thalweg unit and is overall finer grained. Medium-scale cross-beds of the Gt, St_g, St_c and rarely the Sp facies compose sets of inclined bedsets (large-scale inclined strata sets). The top surface is commonly an erosional base of the overlying conglomerate of thalweg fill, however, gradational transitions to the mudstone unit are also observed. The thickness of inclined units averages 3.8 m with lengths usually less than 100 m normal to paleoflow. Large-scale inclined strata sets display upward decreasing grain sizes, however some of them show little vertical grain-size variability (Fig. 5).

Bedsets (*sensu* Bridge 1993b) are equivalent to lateral accretions bounded by 2nd order surfaces of Allen (1983) and stratum bounded by 3rd order surfaces of Miall (1988, 1996). Inclined bedsets consist of cross-beds of similar lithofacies. Most bedsets are composed of medium-scale cross-beds of pebbly sandstone (St_g facies) and conglomerate (Gt facies) that display tangential and less commonly sigmoidal trough-cross stratification (Fig. 3E). Gradational gravel-sand segregation and random openwork cross-laminations are commonly observed. Bedset inclinations vary vertically and laterally within strata sets (5–20° relative to the basal contact) and display a wide range of dip directions that vary from downstream, normal, to upstream, to regional paleoflow. Most bedset bounding surfaces are erosional and gently inclined (< 15°) and commonly display planar, concave-up and rarely convex-up shapes. Simple large-scale inclined strata sets of the St_g facies fill also concave-up channel shape bodies (large-scale troughs) that display gradational gravel-sand cross-bedding (Fig. 3A). Planar cross-beds (facies Sp) are rarely observed but form thick inclined bedsets comprising tens of meters wide strata sets (Fig. 3D). Large-scale inclined strata sets display a number of internal discontinuities and/or disconformities

Figure 3. Photographs of lithofacies. • A – scour base of planar cross-stratified cobble conglomerate (Gp facies) with large mudstone rip-up clasts composing a lenticular thalweg unit of the G channel-bar system. This thalweg unit cuts through a simple set of large-scale strata (St_g facies) forming a large-scale trough. Note gradation within individual cross-beds; hammer for scale. • B – planar cross-stratified conglomerate (Gp facies) with locally weakly developed gravel-sand couplets. Note the cobble lag at the top of the conglomerate unit capped by sandy bedform (St_g facies). Scale bar at Fig. 3B–F is 2 m. • C – composite thalweg unit at the base of the channel belt 4 consisting of the basal cobble conglomerate of the Gm facies overlying 6th order channel belt bounding surface, and sets of trough cross-stratified conglomerate (Gt facies) and cobble conglomerate of Gm facies at the top that overlie the 5th order channel bounding surface marking the boundary between M and N channel-bar systems. • D – simple sets of planar cross-stratified sandstone (Sp facies) form solitary sheet-like bodies, E channel-bar system. • E – large-scale inclined strata of the K channel-bar system consisting of medium-scale trough cross-stratified sandstone and conglomerate (St_g and Gt facies). • F – erosional relic of trough-cross stratified clayey sandstone (St_c facies) sharply overlying basal gravel lag at the top of the inclined unit. • G – medium-scale trough cross-beds of St_h facies that fill a channel shape body incised into floodplain mudstone; top of channel belt 5. • H – erosional relic of tabular mudstone (Fl facies) sharply overlying massive conglomerate of the Gm facies with imbricated pebbles at the top of a composite thalweg unit of the C channel-bar system. • I – fine wedge-shape aggregate structure accompanied by circular to vermicular yellow mottles in the Bss2 horizon of the type I paleosol (Vertisol); lower boundary is a slicken plane. • J – vertical bifurcations of root halos accompanied by redox-depletions and weak medium wedge-shape aggregate structure in the 2Bss2 horizon of the type II paleosol (Vertic Protosol).
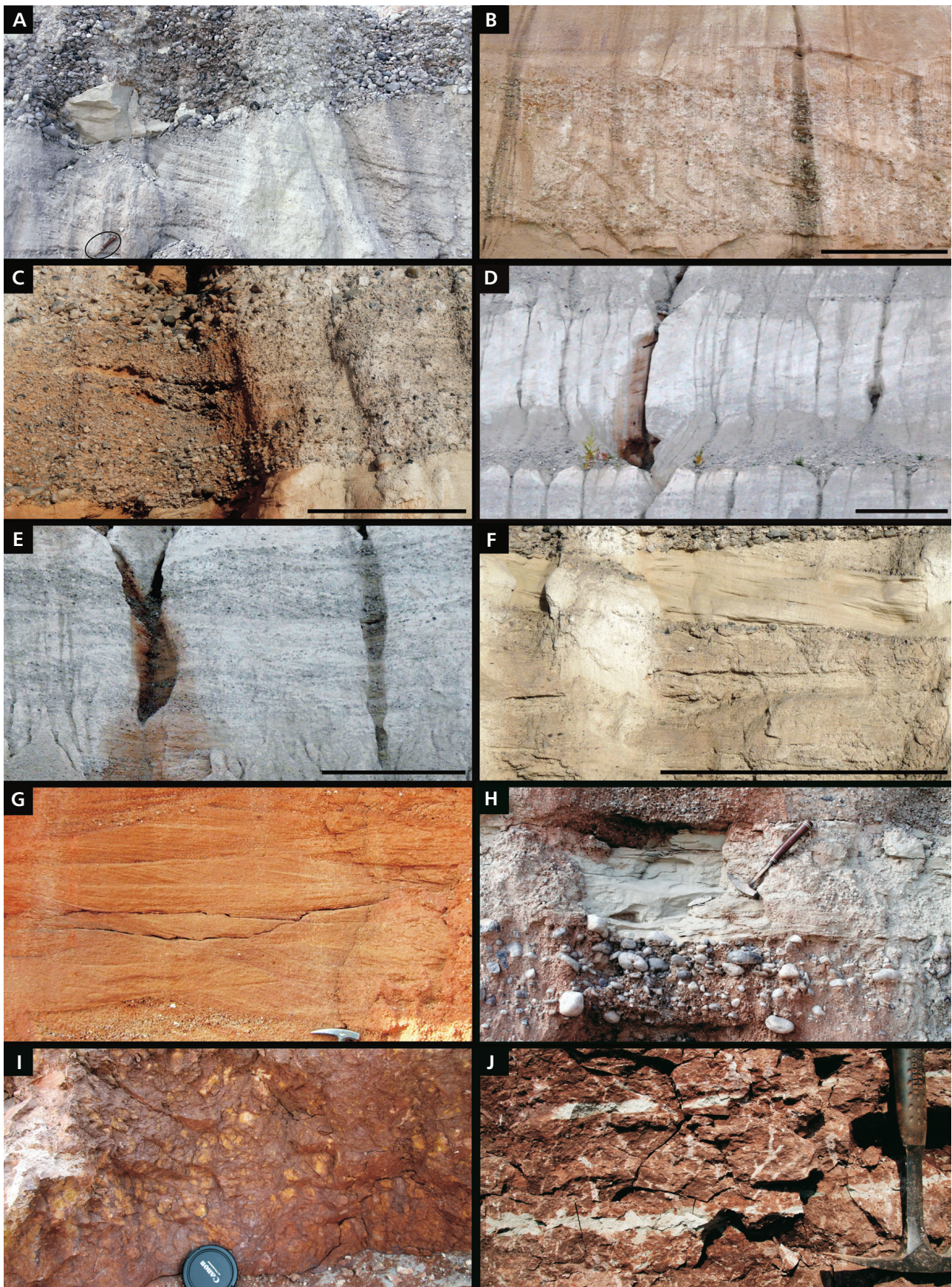
Table 1. Description and interpretation of lithofacies.

Facies	Lithology	Sedimentary structures	Geometry	Interpretation
Gm	Well sorted, clast supported cobble conglomerate (Fig. 3A, C), 10–40 cm clast size, mudstone rip-up clasts up to 1.3 m	Massive, crude horizontal to low-angle (< 10°) cross-bedding, openwork structure, scour surfaces, local clast imbrication	Extensive sheets (> 100 m wide) or lenticular bodies, average bed thickness is 0.43 m (< 1.9 m), planar, locally scoured bases	Diffuse bedload sheets deposited from the highest-energy flows at the deepest part of alluvial channels
Gp	Moderately to poorly sorted, clast supported coarse grained to cobble conglomerate (Fig. 3B), 3–20 cm clast size, varying amounts of coarse sandy matrix, mudstone rip-up clasts < 0.5 m	Planar cross-bedding (< 25°), large-scale simple sets display gradational gravel-sand couplets, bimodal and openwork gravel in cross-beds	Sheets of large-scale planar sets (< 100 m wide, < 2.4 m thick), average cross-bed thickness is 0.95 m, planar to concave-up bases	Bedload deposition from high-energy flows forming straight-crested dunes and unit bars at the deepest parts of alluvial channels
Gt	Well to moderately sorted, clast supported fine grained to pebble conglomerate (Fig. 3C), 1–8 cm clast size, mudstone rip-up clasts < 0.2 m in diameter	Tangential trough cross-bedding, solitary large-scale troughs, bedsets comprise medium-scale cross-beds of well sorted and sandy conglomerate	Large-scale solitary troughs (< 20 m wide, < 1.3 m thick) or sheet-like bedsets (< 2.6 m thick) comprising cross-beds of average thickness 0.53 m, concave-up to undulating bases	Bedload deposition under high-energy flow conditions from migrating curved-crested dunes, minor channel fills and scour fills
St$_g$	Moderately to poorly sorted, coarse to granule-grade sandstones with common pebble admixture (Fig. 3A, E), locally heterolithic with alternating coarse to fine sandy and silty laminae, encompass Gt facies cross-beds	Tangential trough cross-bedding, large-scale solitary sets with graded gravel-sand couplets, bedsets comprise also gravel troughs, wedges or discontinuous sheets	Large-scale solitary troughs (< 30 m wide, < 1.8 m thick), cross-beds stack to lenticular inclined bedsets (< 3.5 m thick), average cross-bed thickness is 0.43 m, concave-up to undulating bases	Bedload deposition under high- to moderate-energy flow conditions from migrating curved-crested dunes, minor channel and scour fills
Sp	Moderately sorted, coarse to granule-grade sandstone with pebble admixture and laminae (Fig. 3F)	Planar cross-bedding (< 30°), large-scale simple sets	Simple sets form sheet-like bodies (> 50 m wide and up to 3.5 m thick), average cross-bed thickness is 1.3 m	Straight-crested dunes and bars, delta-like lobes overgrowing bars, possible confluence zones
St$_c$	Moderately to poorly sorted, fine to medium grained sandstone (Fig. 3G), rich in muddy matrix, common occurrence of silicified tree trunks up to 18 m in length and 0.7 m in diameter	Tangential trough cross-bedding, low-angle cross-bedding (< 10°) or plane beds, rare ripple cross-lamination, heterolithic with thin clay interbeds, in places massive with common burrows	Lenticular bedsets (< 50 m wide and < 2 m thick) are composed of cross-beds of average bed thickness 0.54 m (< 1.5 m), gradational or sharp base and erosional top	Mixed bedload and suspended load deposition from relatively lower-energy flows forming migrating curved-crested dunes and low amplitude bed waves
St$_h$	Poorly to moderately sorted, coarse to fine grained sandstone, heterolithic, locally pebbly (Fig. 3H) with variable portion of muddy matrix	Tangential cross-bedding locally disrupted by burrows, heterolithic with overall fining upward grain-size	Concave up channel shape bodies (< 30 m wide, < 3 m thick) incised in mudstone units, average cross-bed thickness is 0.12 m (< 0.4 m)	Mixed suspended and bedload deposition in alluvial plain channels representing either crevasse or floodplain channels
Fl	Mudstone and siltstone with fine to medium grained sandstone laminae (Fig. 3H), thin greenish grey sheets and reddish brown tabular units	Horizontal to wavy lamination locally disrupted by burrows, root halos, graded sandstone laminae, floral impressions (*Cordaites, Calamites*)	Simple horizontal sheets (< 50 m wide, < 0.9 m thick) or complex tabular units (> 1 km wide, < 15 m thick); sharp to gradational base	Deposition from suspension in standing or slowly moving body of water in abandoned channels and floodplain lakes
P	I. Massive mudstone, well developed horizonation, high-chroma colours, iron-oxide concentrations and nodules (Fig. 3I)	Slickensides and fine–coarse wedge shaped aggregate structure (WSA), mottling	Extensive sheets (> 300 m), up to 1.4 m thick, gradational base, sharp to erosional top	Vertisol developed on distal floodplain reflecting prolonged period of surface exposition
	II. Massive mudstone, moderately to poorly developed horizonation, high-chroma colours, iron-oxide tubules and concentrations in matrix (Fig. 3J)	Slickensides and weak fine-medium WSA, relic lamination, root traces cemented with iron-oxides, bifurcating root halos with redox depletions, mottling	Extensive sheets (> 300 m), up to 3.5 m thick, sharp base, erosional top	Compound paleosol sequence of Vertic Protosol and Protosol developed on medial to proximal parts of aggrading floodplain

associated with changes in grain size, cross-bed geometry and dip direction.

Fine to medium grained, sandy cross-beds (St$_c$ facies) with tangential trough-cross to low-angle cross (< 5°) and planar stratification comprise the upper portions of inclined strata sets (Fig. 3F). They typically have sharp basal contacts and stack laterally to form lenticular bedsets that display inclined cross-bed bounding surfaces dipping normal, to downstream, to paleoflow direction. Pebbles are concentrated within the lower axial parts of some cross-beds and disappear upwards and laterally in cross-laminations. Silicified tree trunks are commonly observed in this facies and are oriented either parallel, or perpendicular to, cross-bedding axes. Thin
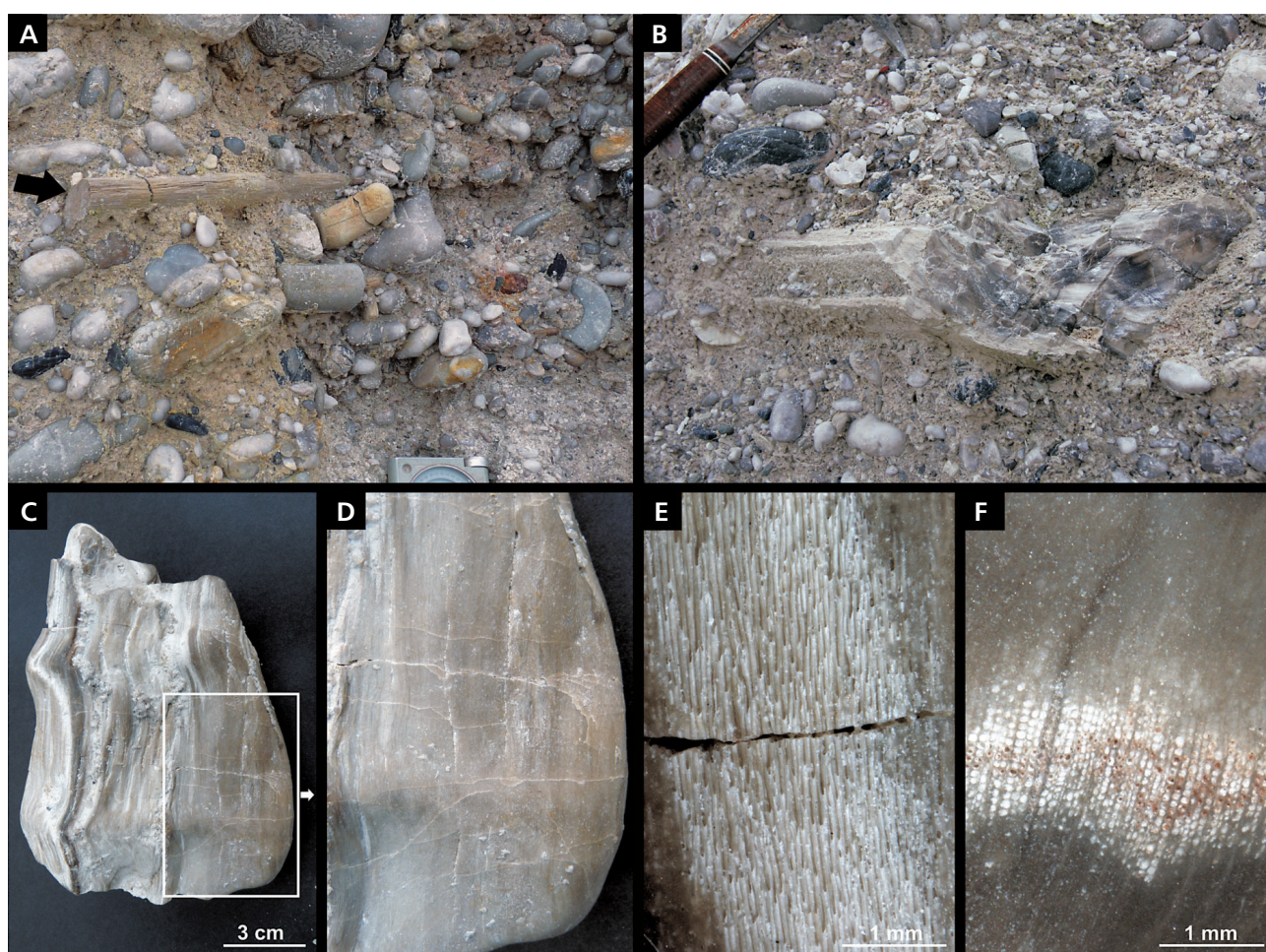
Figure 4. Silicified tree trunk deposited in conglomerate of thalweg fills. • A – part of a tree branch (arrowed) transported in wooden state and silicified *in situ* (Gt facies). • B – part of tree trunk transported in wooden state and silicified *in situ* (Gp facies). • C, D – well-rounded cobble of silicified tree trunk that displays smooth surfaces, possibly indicating bedload transport and reworking of previously silicified tree trunk. • E, F – tracheids partly filled by kaolinite indicating the wooden origin of the cobble.

sheets and drapes of mudstone (Fl facies) locally cap inclined strata.

Interpretation. – Large-scale inclined gravel-sand and sandy strata are interpreted as barforms and channel fills. Large-scale inclined strata (bedsets) represent seasonal accretionary barform elements reflecting individual flooding events (Bridge 1993a, b; Willis 1993). The composite nature, internal structure and facies composition appear similar to that of compound braid bars (Lunt *et al.* 2004). The most complete units display upward decreasing grain sizes and set thicknesses indicating preferential preservation of the downstream parts of barforms (Bridge 1993b).

Medium-scale tangential trough cross-beds reflect migration of curved crested gravel-sand dunes that cover lower bar accretional surfaces (Gustavson 1978, Miall 1996, Best *et al.* 2003), whereas sigmoidal trough cross-beds and planar cross-beds reflect avalanche surfaces of unit bars (Bridge 1993b, Bridge & Tye 2000). Large-scale sets of exceptionally thick planar cross-beds represent chute and tributary mouth bar surfaces or delta lobes at channel confluence zones (*e.g.*, Bristow & Best 1993; Bridge 1993a, b; Ullah *et al.* 2015). Smaller scale concave-up channel shape bodies filled by simple sets of large-scale inclined strata (Fig. 7, Appendix) represent cross-bar channels (Bridge & Tye 2000). Clay rich sandy bedsets with muddy drapes represent relics of sigmoidal dunes and low amplitude bed waves deposited at shallow areas of upper bars, locally preserving upper plane bed flow conditions. Where these cross-beds overlie concave-up erosional surfaces they probably represent abandoned channel fills. Both cases reflect deposition from mixed bedload and suspended-load streams of decreased stream-flow capacity likely at elevated parts of channel belt.

Orientation of barform accretional directons range from normal to parallel to the regional paleoflow. Paleocurrent data from medium-scale cross-beds integrated with dip directions of related inclined surfaces display angles ranging from 10 to 100° (locally these angles can exceed 100°). Variability of less than 60° between the bar accretion direction and paleocurrent indicators are typical for bar growth downstream, or oblique to, local flow, whereas greater values are interpreted to represent lateral accretion (Miall 1996). Locally, potential upstream accretional surfaces are also observed.

The preserved bars may also give an indication of paleoflow depth. Lower bar accretion surfaces onlap or pass into underlying thalweg deposits suggesting that the barform flow depth should be measured from the base of the underlying thalweg fill to the top of the fine grained bar top assemblage. The mean flow depth, as estimated from 26 barforms, ranges from 4.3 m to 6.3 m. The bar tops are truncated by an overlying thalweg unit; thus, these estimates should be considered minimums.

Mudstone units

Description. – Mudstone units constitute a minor part of the studied succession (< 10 %) and form either simple thin horizontal sheets (< 0.9 m) of confined lateral extent (< 100 m) or complex thick tabular units (< 15 m) extending for several kilometres. The simple thin sheets consist of laminated mudstone to siltstone (facies Fl) that may contain cm-thick, graded, medium to fine grained sandy laminae. The complex units are composed of laminated mudstone to siltstone (facies Fl), paleosols (facies P, Fig. 3I, J) and concave-up sandstone bodies (facies St_h). Mudstone units display sharp or gradational bases and erosional upper boundaries. The simple horizontal mudstone sheets usually cap inclined strata; however, they also can be interbedded in sheet-like conglomerates of thalweg fills (Fig. 3H). Simple mudstone units up to 0.5 m thick can also overlie inclined (< 20°) accretional surfaces of barforms or rarely fill concave-up channel shape bodies (Fig. 8).

The complex mudstone units overlie inclined strata and are cut by prominent erosional surfaces overlain by conglomerate sheets of thalweg fills. They contain paleosols of variable maturity, composition and thickness (see below). Concave-up sandstone bodies (facies St_h) are rarely encased within mudstone units and form channel shape bodies at least 30 m wide and up to 3 m thick that have basal conglomerate thalweg fill and a steep cut bank (Fig. 8). They dominantly consist of medium grained sandy cross-beds, up to 0.4 m thick, that display tangential trough-cross bedding (Fig. 3G). Cross-beds form gently inlined (< 5°) bedsets that become finer upwards as a result of an increasingly muddy matrix. Gradational tops into mudstones are disrupted and mottled with root halos.

Interpretation. – Thin and laterally confined sheets of laminated mudstones with graded sandy laminae are interpreted to have been deposited from suspension in a standing or slowly moving body of water. They are interpreted to represent erosional relics of abandoned channel fills formed in local topographic lows during periods of low flow or abandonment of mainstream channels. Thick and laterally continuous complex mudstone units with paleosols and incised channel sandbodies are interpreted to represent floodplains that were kilometers across. Laminated mudstones record deposition within shallow ponds on floodplains. The presence of roots and local disruption by burrows indicate that the ponds were shallow enough for bottom sediments to support plants (Willis 1993). Paleosols record surfaces that received minimal deposition for prolonged periods of time in distant floodplain environments. The concave-up sandstone bodies are interpreted to represent fluvial channels crossing the ancient floodplains. Relatively small and shallow channels were dominantly filled by bedload deposits with periods of mixed suspended and bedload deposition. They probably represent mainstream rather than crevasse channels as evidenced by their complex internal architecture. The rarity of complex mudstone units within the fluvial strata is attributed to erosion by channel incision, lateral migration and depositon of overlying thalweg units.

Stacking patterns and cyclic hierarchy

The alluvial architecture is characterised by vertically stacked conglomerate sheets of thalweg fills and inclined gravel-sand and sandy strata of barforms with subordinate floodplain mudstone. These architectural components stack to form a hierarchy of cyclical packages. The smaller scale cycles are interpreted to reflect autogenic processes of channel migration in the active channel belt. Channel migration cycles represent the passage of individual channel-bar systems that filled and modified the main channels. Channel-bar systems represent erosional relics of channel elements and their stacking patterns reflect channel behaviour (Figs 6–8). They stack vertically and laterally in channel belts, which are sheet-like units bounded by extensive erosional surfaces representing regional avulsion events (Heller & Paola 1996). At a larger scale, multiple channel belts stack vertically into packages of alternating thalweg-dominated and barform-dominated zones lacking preservation of floodplain mudstone. The processes responsible for the formation of these large-scale stacked channel-belt complexes are uncertain, however they may be attributed to allogenic controls that commonly operate at this scale (*e.g.*, Olsen *et al.* 1995, McLaurin & Steel 2007).
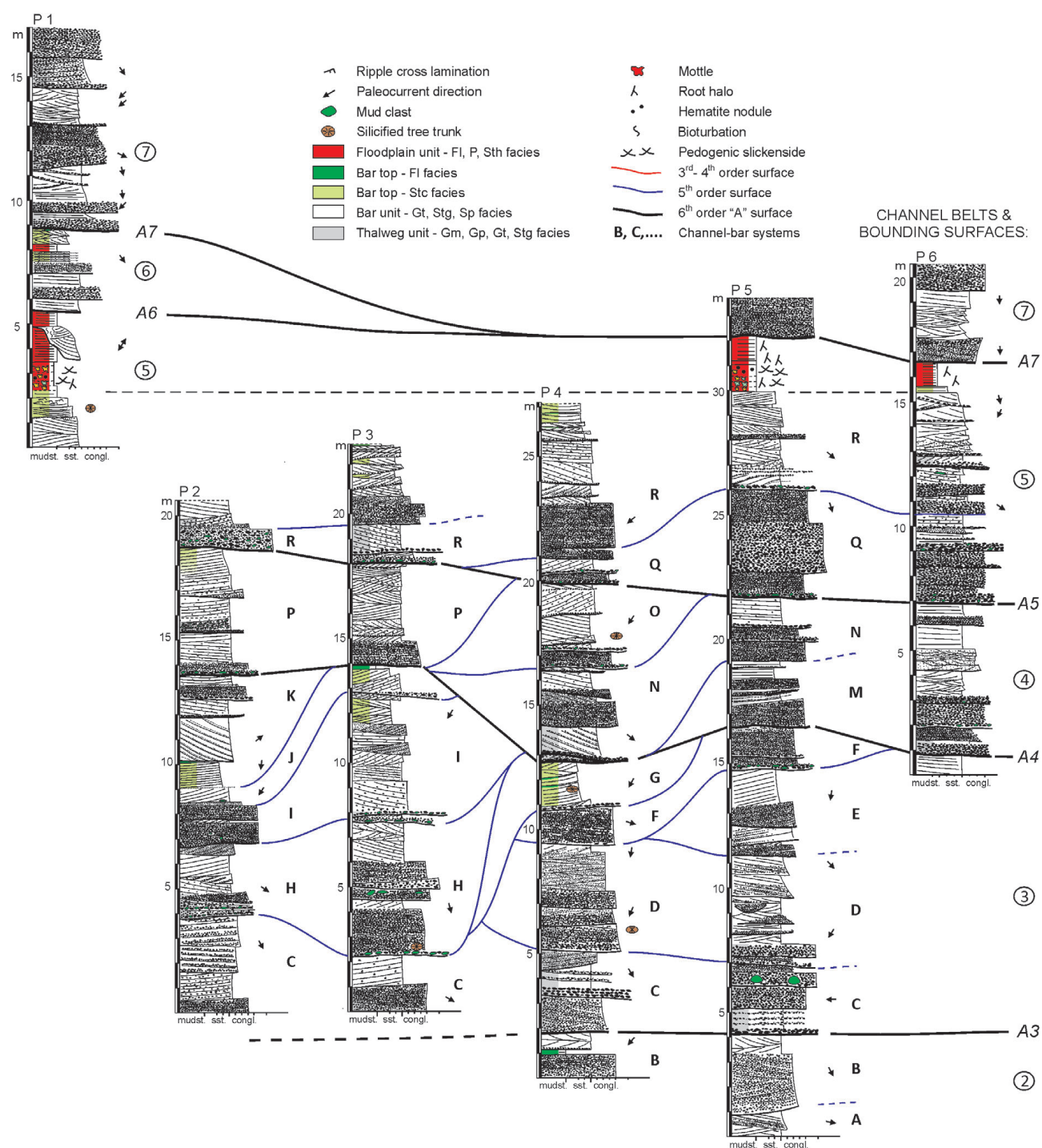
Figure 5. Measured sections showing vertical facies patterns, architectural components and paleoflows (N to the top) of individual channel-bar systems (capital letters) that make up channel belts bounded by prominent 6th order bounding surfaces (termed A1–7). See Figs 2 and 7 for the position of the measured sections.

Channel-bar systems

The aforementioned architectural components should ideally stack vertically to form a fining upward package of a single channel-bar system (CBS) consisting of a basal conglomerate of a thalweg fill, which is overlain by inclined strata of barforms that pass upwards into floodplain mudstone. This pattern would be similar to the fining upward succession described by Allen (1983) that represents the migration and filling of a channel followed by abandonment and

establishment of floodplain deposition. In a dynamic system such as a fluvial environment, preservation is a critical factor that will directly impact the resulting alluvial architecture (Siegenthaler & Huggenberger 1993, Lewin & Macklin 2003). The amalgamated nature of the fluvial deposits rarely allows the complete preservation of a single channel-bar system. Rather, they stack vertically without preserving individual bar and floodplain components of each channel-bar system and produce the composite thalweg units, which represent the topographically lowest part of the system (Siegenthaler & Huggenberger 1993). Some composite thalweg units may include discontinuous drapes of abandoned channel fill deposits and/or grade laterally to a suite of conglomerate sheets of single thalweg fills that encase several inclined strata sets of lower bar deposits (C and northern continuation of Q CBS, Fig. 7). The composite nature of these thalweg bodies indicates generation by repeated migration of channel-bar systems under low rates of aggradation (Miall 1980, McLaurin & Steel 2007). The maximum observed thickness of composite thalweg units reaches 4.3 m and averages 2.1 m. The thalweg units pass upwards into the inclined strata of barforms that locally preserve fine grained upper bar or abandoned channel deposits at their tops. Channel-bar systems with simple thalweg fill and associated barform may stack vertically into large channel shape bodies (J and K CBS, Fig. 7). The maximum bankfull channel depth can be estimated from the thickness of the channel-bar system. The thickness of 33 channel-bar systems measured from the base of the composite thalweg fill to the top surface of barform averages 6 m with a maximum of 10 m.

Channel-bar systems overlie erosional surfaces of planar shape and lateral extent exceeding 200 m where they are oriented parallel to paleoflow. In sections normal or oblique to paleoflow, most have concave-up geometries, lateral extents ranging from 30 to 100 m and significant erosional relief of up to 8 m (Fig. 5). Except for rarely irregular and scoured surfaces covered directly by inclined strata of lower bar deposits (B CBS, Fig. 7), most of these bounding sufaces are overlain by simple or composite thalweg fills. These channel-bar system bounding surfaces correspond to 5th order surfaces of Miall (1996) and 3rd order surface of Allen (1983) bounding large channel forms. The lower, 4th order surfaces record the main erosional and accretional events of individual channel-bar systems and correspond to the 4th order surfaces of Miall (1996). They have inclined ($< 10°$), concave- or convex-up shapes with relief up to 3 m and a lateral extent up to 50 m.

Channel-bar systems appear to be similar to alluvial stories defined as the deposit of a single channel-bar and adjacent channel fill (Friend *et al.* 1979). They represent relics of formative channels stacked laterally and vertically in a channel belt. Autogenic processes of channel avulsions, lateral migration, filling and abandonment most

likely controlled the formation of these smallest scale fining upward cycles. Lateral channel migration associated with local avulsion in active channel belts would result in repeated reoccupation of older channels and removal of upper barforms leading to preferential preservation of younger units overlying deeply truncated lower members (Heller & Paola 1996, Lewin & Macklin 2003). Similar patterns of composite thal wegs with a more complete uppermost succession preserved are described in the Morrison Formation as channel-scale sequences (Godin 1991), and channel-bar systems in the fine to medium grained sandy fluvial strata of late Cretaceous Lower Castlegate Formation (McLaurin & Steel 2007).

Channel belts

Channel belts represent areas where river channels laterally and aggradationally deposit primarily sandy and gravelly channel and bar sediments for significant periods of time between major extra-belt channel avulsions (*e.g.*, Bridge & Leeder 1979, Miall 1996). Within the Nýřany Member, a channel belt is described as a succession from a composite thalweg unit overlain by a barform, which may be in turn overlain by overbank deposits. These sheet like fining upward packages extend laterally for hundreds to thousands of meters and are separated by prominent erosional surfaces that are interpreted to record regional avulsion events (Heller & Paola 1996). Channel belts contain a number of laterally and vertically stacked channel-bar systems; there are usually two to four channel-bar systems stacked within the thickness of a channel belt. The thickness of channel belts varies usually from 4 to 14.5 m.

Channel belt bounding surfaces display a planar, gently undulating shape with shallow scours and relief up to 5 m over a distance of about 300 m (A1–A7, Figs 5–8). They are overlain by composite thalweg units and have significant lateral extent (> 1000 m). They form low-relief planar composite surfaces both normal, and parallel to the paleoflow and most likely represent 6th order surfaces (Miall 1996, Holbrook 2001). Excluding A1, A6 and A7 that incise floodplain mudstone units, all of the observed surfaces cut into fine grained upper bar assemblages. The former surfaces cutting through floodplain mudstone typically have basin-wide lateral extent and bound stacked channel-belt complexes (see below).

The lowermost observed channel belt (CB1) is poorly exposed and cuts a floodplain mudstone unit on the floor of the Kaznějov quarry (Fig. 6). It consists of large-scale inclined strata set with partially preserved upper bar deposits that are cut by a planar erosional surface (A2). The overlying channel belt (CB2) is composed of four vertically stacked channel-bar systems that, with the exception of the basal composite thalweg unit, preserve mostly inclined strata sets. The lower inclined strata set records a down-

stream accreted lower bar cut by a cross-bar channel (left side, Fig. 6) and capped by a bar top assemblage of abandoned channel fill. Similar associations with laterally accreted lower and upper bar deposits are characteristic of the overlying channel-bar system (A CBS, Fig. 7). Above, there are laterally accreted lower bar and associated channel fill deposits that overlie a scoured concave up surface (B CBS, Fig. 7). It is cut by a prominent erosional surface (A3) overlain by a composite thalweg unit of the following channel belt (CB3).

The most complex observed channel belt CB3 is made up of ten vertically and laterally stacked channel-bar systems exposed in outcrop (C–L CBS, Fig. 7). An extensive basal composite thalweg unit (C CBS) consists of vertically stacked gravel sheets and laterally adjacent scour fill and lower bar deposits. The overlying channel-bar systems are composed of a nearly complete fining upward packages of thalweg fills passing upwards to inclined strata with relics of upper bar deposits at the tops. They cut each other and tend to be inclined (up to 10°) to the south-east and south-west reflecting translation of formative channels (*e.g.,* F, G, I, J and K CBS, Fig. 7). The lower D channel-bar system preserves laterally accreted lower bar deposits, erosional relics of cross-bar channel (left) and upper bar deposits. The above large-scale strata sets of the E channel-bar system probably represent a tributary mouth bar deposit formed at the confluence zone of northwestern and northern anabranch channels. It is overlain by a relic of a composite thalweg unit of the F channel-bar system, which is laterally cut by the G channel-bar system preserving deeply incised lenticular thalweg fill with mudstone rip-up clasts accumulation that pass upwards to inclined strata of lower and upper bar deposits. It is cut by the composite thalweg unit of the following sheet-like channel-bar system (H CBS, Fig. 7) that is composed of laterally stacked lenticular thalweg fills locally preserving mud clast accumulation along the cut bank. The J and K channel-bar systems stack vertically into a large channel shape body, which is deeply incised up to the composite thalweg at the base of the channel belt (Fig. 7). This channel body formed during maximum bankfull flow and was subsequently filled by the two vertically stacked channel-bar systems most likely recording mean flow depths. Muddy sandstone (St_c facies) preserved at channel margins above the concave-up incision surface indicates temporal channel abandonment following incision. Both channel-bar systems display basal lenticular thalweg fills that become thicker towards the cut bank. The overlying inclined strata preserve lower bar accretional surfaces that pass to laterally accreted scroll bar increments capped by upper bar deposits (J CBS, Fig. 7). The passage and deposition of younger K channel-bar system further expanded the formative channel. It is cut by the planar inclined surface recording lateral southern ward translation of active channel
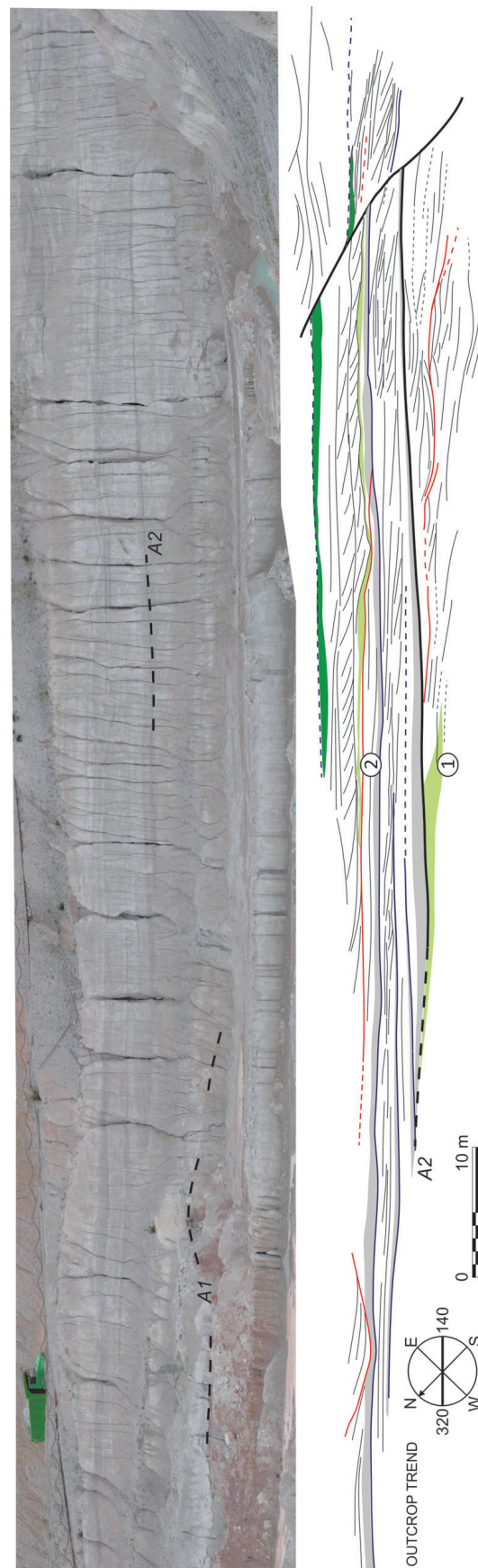

Figure 6. Photopanel of the lowermost part of the Kaznějov quarry showing lower channel belts 1 and 2. Poorly exposed lowermost channel belt cut into underlying floodplain unit and is built mainly by inclined strata of barforms. The above channel belt 2 begins with several vertically stacked sheets of conglomerate that laterally stack into a composite thalweg unit. Overlying inclined strata fine upwards indicating a nearly complete preservation of barforms.

under a consistently eastern to southeastern paleoflow direction.

The A4 channel belt bounding surface cut through the E to L channel-bar systems but became less evident south ward. It is overlain by a composite thalweg unit that also wedges out to the south possibly indicating a transition to a more peripheral zone of the active channel belt (CB4) as supported by common cross-bar channel deposits. Individual sheet-like channel-bar systems are stacked laterally and bounded by gently inclined surfaces diping to the south. The overlying channel belt (CB5) is composed of a thick composite thalweg unit that thickens northward where it encompasses several inclined strata sets of downstream and laterally accreted lower bar deposits. The composite thalweg unit pass upwards to south-western inclined large-scale strata sets of lower and upper bar deposits passing upwards to thick floodplain mudstone at the top of the channel belt (Figs 7 and 8). The mature type I paleosol is developed at the lower part of this floodplain unit, which is truncated by a relatively small incising, finer grained channel sand body (Fig. 8). Channel belt 6 that overlies the planar, locally scoured erosional surface (A6) differs from others by the local preservation of associated floodplain mudstone and a minor proportion of thalweg fills (Fig. 8). The lateral stacking of channel-bar systems indicates western translation of the formative channel under a consistently southern to southwestern paleoflow direction. It is completely truncated by the thick composite thalweg of the overlying channel belt resulting in a discontinuous lenticular body.

Stacked channel-belt complexes

Channel belts tend to stack without preservation of floodplain units resulting in a vertical alteration of thalweg fill and barform dominated zones. Nearly all channel belts can have locally preserved relics of floodplain mudstone. However, their patchy distribution and minor thickness imply weak development of original floodplains perhaps due to shorter formation times or lower aggradation rate than that responsible for the formation of complex and laterally extensive floodplain units. These units are up to 15 m thick and can be correlated for several kilometers in sections parallel to the basin axis where they separate a series of thalweg and barform dominated intervals (Figs 9 and 10). The term stacked channel-belt complex is used to describe these intervals that usually represent a series of two to three stacked channel belts and locally perhaps more (Fig. 9). These stacked channel-belt complexes range from 10 m to 35 m thick, are capped by laterally extensive floodplain units, and are separated by large-scale erosional surfaces (Fig. 10). Stacked channel-belt complexes form sheet-like and lenticular sandbodies, later prevailing at stratigraphic intervals of the Toušov, Nýřany and uppermost Chotíkov

group of coal seams. Complex of sheet-like sandbodies below the Nevřeň group of coal seams appear to overlie a prominent surface reaching erosional relief up to 15 m (Fig. 10). Surfaces separating sandbodies may correspond to the 7th order surfaces of Holbrook (2001) that bound nested valleys composing two to ten channel belts, or to the prominent "S" surfaces of Leleu *et al*. (2009) that extend laterally for tens of kilometers and separate up to 36 m thick braidplain mega-units in a coarse-grained proximal braided fluvial setting. These units are interpreted to reflect allogenic processes such as changes in discharge driven by climate fluctuations or tectonic tilting affecting accommodation space (López-Gómez & Arche 1993). The preservation of thick, basin-wide floodplains in such a dynamic fluvial environment implies an even higher original thickness and thus represents significant aggradational events allowing for the preservation of thick and basin-wide floodplains.

Paleocurrent directions and provenance

Paleocurent directions vary by up to 180° between individual channel-bar systems of a particular channel belt as well as between individual channel belts (Fig. 7). The mean paleocurrent direction for all channel belts is 179° indicating major transport to the south with a circular standard deviation of 74°. The distribution of paleocurrent directions by architectural component indicates two distinct modes of flow direction to the southeast and southwest (mean 191°) for thalweg units compared to a wide range of paleoflow and accretion directions within the bar units (mean 166°). Bar units exhibit a higher circular standard deviation of 77° versus 48° for the thalweg units.

Clast composition is mature predominantly consisting of sub rounded to rounded quartz, laminated sedimentary quartzite, likely of Ordovician origin, and massive to laminated black chert likely of Neoproterozoic origin; subordinate components present include kaolinite-altered rhyolitic volcanics, quartz cemented coarse-grained lithic breccia and sandstone. Sandstone pebbles consist of quartzarenite with angular grains and variable degrees of sorting. Sub-rounded cobbles of silicified tree trunks are rarely present in the gravel sheets of thalweg fills (Fig. 4).

Arkosic pebbly sandstones consist of sub angular quartz grains; subordinate feldspars are nearly completely altered to kaolinite. The heavy mineral associations seem to be similar across all of the studied channel belts suggesting no prominent changes in the drainage basin (Table 2). Leukoxene, the weathering product of TiO_2 group minerals (rutile, anatase), is the dominant heavy mineral (20–60%), that may have been formed during long transport and multiple redeposition events and/or also *in situ* after burial. Staurolite, tourmaline, rutile and zircon are common. Ilmenite and kyanite occur subordinately.
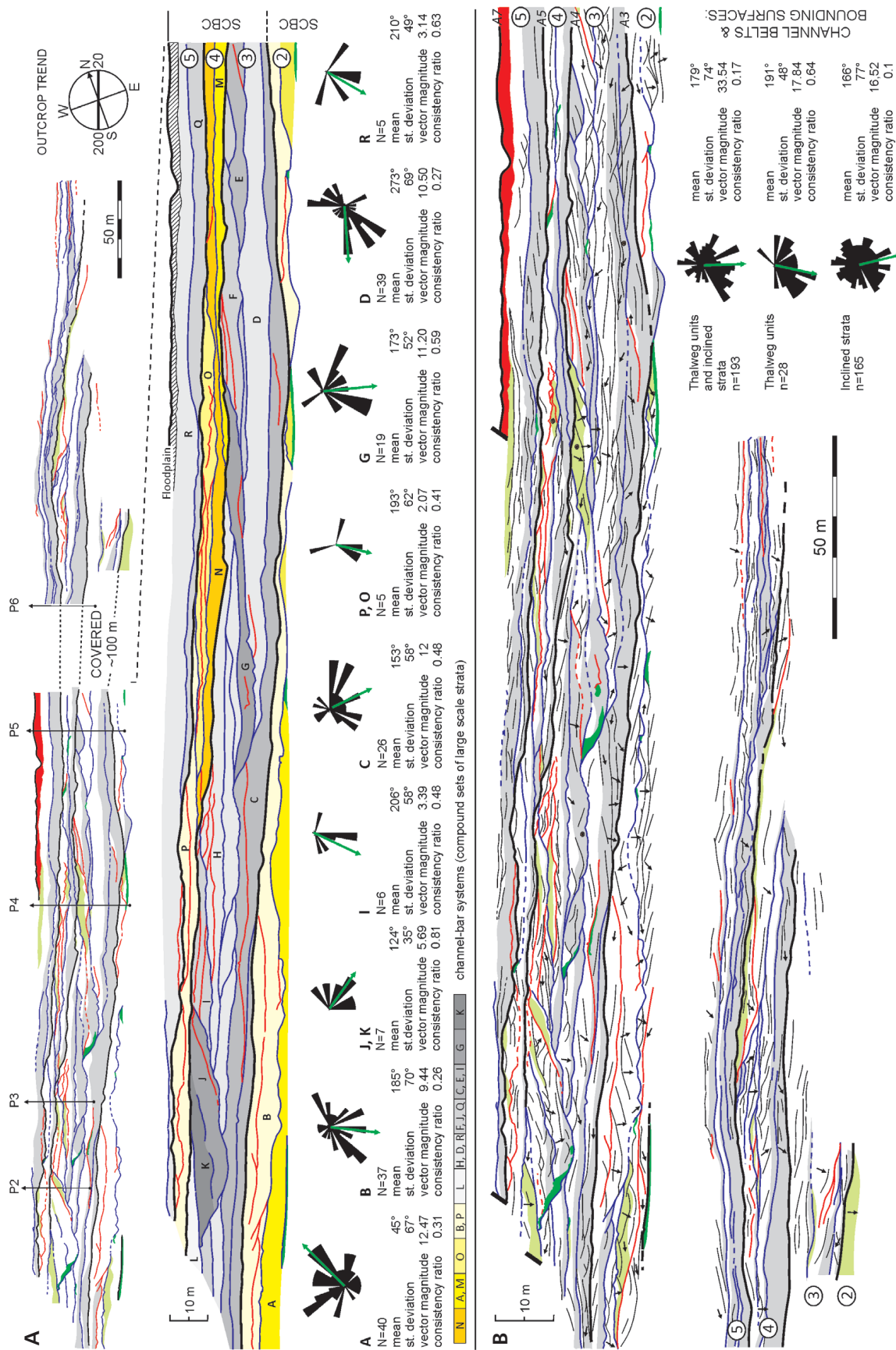
Figure 7. Panel of the western face of the Kaznějov quarry. • A – sketch of the outcrop at the top shows distribution of the main architectural components and position of measured sections; 1.8 vertical exaggeration. Below is an interpretation panel with channel-bar systems (capital letters and color scale), channel belts (circled) and their bounding surfaces (italic) and stacked channel-belt complexes (SCBC) indicated. Paleoflow directions display wide scatter between individual channel-bar systems and channel belts; 1.2 vertical exaggeration. • B – detailed panel of alluvial architecture showing distribution of the main architectural components and large-scale inclined strata. Paleoflow directions are plotted relative to the outcrop (down is out from the outcrop); 1.8 vertical exaggeration. Detailed bedding diagram is shown in Appendix.

Table 2. Heavy mineral associations of sandstones in percent. Rock – rock fragments.

Locality	Sample ID	Amfibole	Anatase	Apatite	Ilmenite	Kyanite	Leucoxen	Magnetite	Rutile	Staurolite	Tourmaline	Zircon	Rock
Horní Bříza	HB 01 base				2		50	< 1	15	5	3	25	
	HB 02		< 1		10		40		5	10	10	25	
	HB 03 top				< 1		50		10	5	10	25	
Kaznějov	KAZ 01 base	< 1	1				35		20	20	20	4	
	KAZ 02	< 1	< 1			2	50		10	15	20	3	
	KAZ 03	1	1			3	30		15	20	20	10	
	KAZ 04		1			4	45		15	10	15	10	
	KAZ 05	< 1				< 1	20		5	15	10	< 1	50
	KAZ 06		< 1	2	3		50		10	5	5	25	
	KAZ 07	< 1			< 1		60		15	5	10	10	
	KAZ 08 top		< 1			1	50		10	25	10	4	

The sandstone composition reflects a mixture of metamorphic and granitic rocks with a significant proportion or proximity of medium-grade garnet-free and staurolite-rich metamorphic rocks in the drainage basin. Staurolite schists that may provide local material are situated about 30 km to the northwest; however, they are also rich in garnet (Žáček & Cháb 1993). The mature clast composition indicates a rather long transport distance and possible up-valley erosion and redeposition of older Carboniferous coarse clastics originally deposited in source-proximal parts, and a partial sedimentary source of early Paleozoic and Proterozoic age.

The Nýřany Member channel characteristics

Based upon outcrop analysis, the Nýřany Member fluvial system has been interpreted to represent mostly low sinuosity and high energy channels of a braided-river plain prone to avulsion and flooding (Opluštil *et al.* 2005, Bashforth *et al.* 2011). The observed architectural properties and facies composition are indicative of a deep perennial braided river system consisting of at least one trunk channel and several associated second order channels. The braided multi-channel pattern is inferred from downstream accreted bar units commonly cut by small-scale cross-bar channels, the presence of confluence zones represented by scour fills and tributary mouth bars, the scarcity of floodplain units and the overall coarse nature of the deposits. Vertical superposition of channel bars and fills indicate high channel connectedness within channel belts. The perennial character is inferred from the size of the channels and related barforms; however, abandoned channel deposits interbedded within thalweg fills impliy highly-seasonal discharge fluctuation, which is supported by common gravel dunes preserved in the thalweg units. However, a somewhat higher sinuosity of formative channels is indicated by a wide range of paleocurrent and accretional directions of bar units (see below).

Channel depth

Mean bankfull flow depths were estimated directly from the thickness of individual bar units (*e.g.*, Bridge & Tye 2000). Flow depths were measured from the top of a barform to the base of the underlying single thalweg fill. The results show that minimum mean bankfull flow depths average 4.3 m with a maximum of 6.3 m (n = 26). Estimated mean flow depths, corrected by a 10% compaction, average 4.7 m with a maximum about 7 m (Etheridge & Schumm 1978). The maximum bankfull flow depth directly estimated from the thickness of channel-bar systems, measured from the base of the composite thalweg fill to the top of barforms, averages 6 m with a maximum about 10 m. Bankfull flow depth after decompaction ranges from 6.6 to 11 m. An alternative method of undirectional flow depth estimation uses average cross-bed thickness to reconstruct dune height, which is related to the mean flow depth (Leclair & Bridge 2001). Dune height is considered approximately three times the mean cross-bed thickness and resulting flow depth is six to ten times the dune height. The average set thickness of 0.43 m (n = 115) results in a mean dune height of 1.52 m that formed in flow depths ranging from 9 to 15 m. This approach results in slightly higher flow depths than those that derived from bar thickness. This is because only erosional remnants of barforms are preserved. Such a flow depth scales with the thickness of channel belt and reflects a rather maximum bankfull flow depth, which is usually approximately twice the mean flow depth (Bridge 1993b).

The floodplain channel body displays a significantly lower thickness reaching about 3 m in outcrop. The average set thickness of the St_h facies filling this floodplain channel (0.16 m, n = 13) results in flow depths ranging from 3.4 to 5.6 m that confirm the outcrop observation.

Channel width

The width of channel bodies are difficult to measure directly from outcrops due to rare preservation of both channel margins, variable orientation of channels and modification by channel processes after deposition. The only erosional relic of a channel body preserved in section normal to paleoflow (J and K CBS, Fig. 7) is about 60 m wide resulting in a minimum width/thickness ratio of 10 that would classify this channel body as a broad ribbon potentially up to the narrow sheet (Gibling 2006).

To estimate the actual widths of trunk channels an empirical regression equation was used that incorporates mean bankfull channel depth developed by Bridge and Mackey (1993b). Using the mean bankfull flow depth range of 4.7–7 m, which was derived from the thickness of bar units and corresponds to one half of the maximum bankfull flow depth, the resulting channel widths is estimated to be 147–306 m. Using the same equation the predicted widths of floodplain channels range from 80 to 200 m. Empirical equations estimating widths of active channel belt based upon the mean bankfull flow depth typically have large standard errors with braided channel belts widths shifted towards higher values. Using the method of Bridge & Mackey (1993b) the predicted mean channel belt widths range from 970 to 2760 m and provides reasonable grounds for correlation of closely spaced well-logs (Figs 9 and 10).

Channel sinuosity

The sinuosity of ancient channels can be indirectly estimated from dispersion of paleocurrent data as inferred from observations of fractal properties of modern rivers. Ghosh (2000) established a functional relationship between sinuosity of model fractal patterns of simulated channels and dispersion (consistency ratio) of their segment orientations (paleocurrents). The sinuosity is estimated based on calculating the consistency ratio, which is derived from the vector magnitude. Although it was designated for channels, whose sinuosity was steady over time, *e.g.* bank-stabilized non-migrating channels, it has been succesfluly used for low to intermediate sinuosity streams (McLaurin & Steel 2007). Since barform accretion and associated paleocurrents can by highly variable in both meandering and braided streams, paleocurrents taken from thalweg fills were used to calculate sinuosity. Using the methods of Ghosh (2000), the sinuosity of channel thalweg fills is 1.5, which would classify the Nýřany Member as deposits of intermediate sinuosity streams (Miall 1996). Sinuosity of individual channel-bar systems of grouped thalweg fill and barform paleocurrent data range from low sinuosity (1.2, channel body composed of J a K CBS, Fig. 7) to high sinuosity streams (3.5–4.1, A and B CBS, Fig. 7). These high sinuosity channel-bar systems differ from others also by
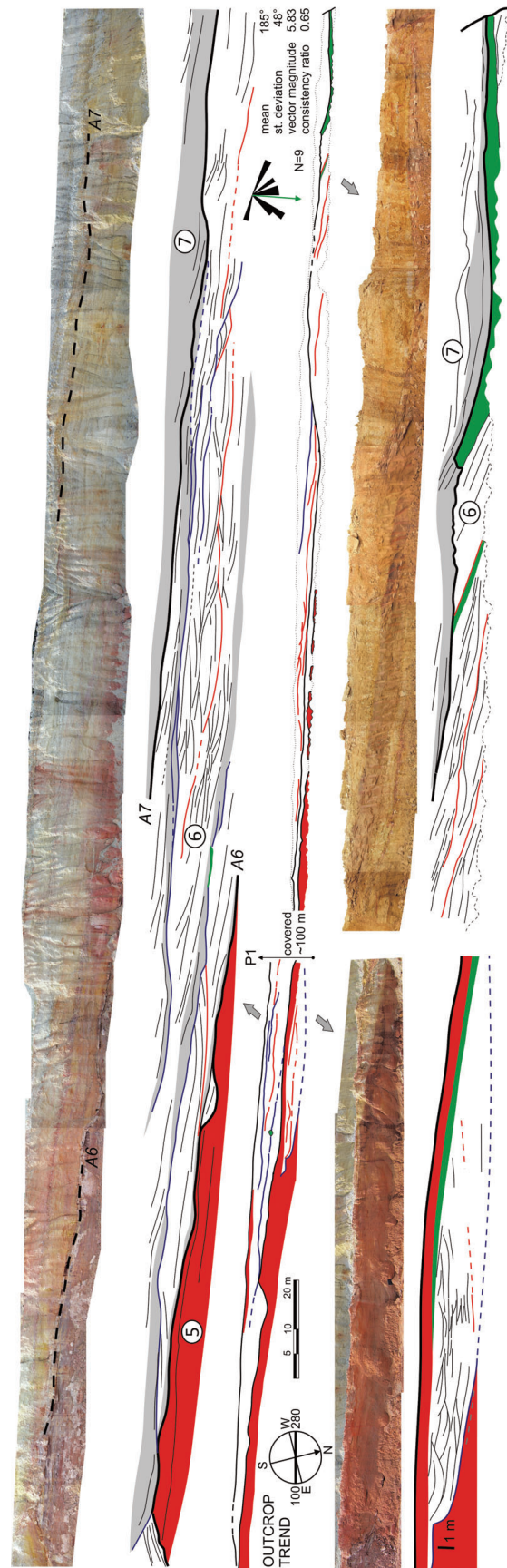

Figure 8. Photopanel of the southern face at the upper part of the Kaznějov quarry above the floodplain unit at the top of the channel belt 5. The channel belt 6 consists of dominantly sandy inclined strata with only minor conglomerate sheets at their bases and displays western lateral channel shifting, lateral accretion of inclined strata and partly preserved floodplain at its top. The architecture of the floodplain channel is dominated by small medium-scale cross-beds of the St$_h$ facies composing low-angle inclined bedsets.
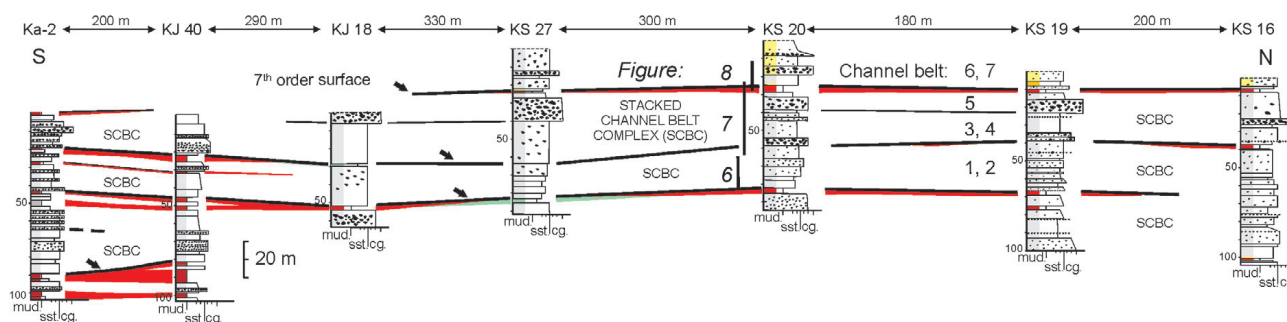
Figure 9. Correlation panel of shallow exploratory wells drilled in the area of the Kaznějov quarry and vicinity that display lateral stability of certain channel belts and stacked channel-belt complexes; the last are bounded by basin-wide 7th order surfaces.

their northeastern paleocurrrent direction (mean 45°) and northwestern oriented accretion surfaces (A CBS). Supporting the idea of intermediate sinuosity, the channel belt preserves a wide range of channel orientations indicated by many highly oblique and side slices of channel-bar systems (Holbrook 2001).

Paleosols

Paleosols are developed in floodplain units at the top of channel belts and stacked channel-belt complexes. Laterally extensive paleosols formed in at least 15 stratigraphic levels in the Nýřany Member deposits. They have variable thicknesses, morphologies, compositions and maturities, and range from peat accumulations represented by Histosols, through gleyed Vertisols with sphaerosiderite and high chroma Vertisols with common slicknesides, to calcic Vertisols containing dolomite nodules (Fig. 11A, B). Most of the paleosol sections are compound or composite (Kraus 1999) type paleosols and display lateral/spatial transitions between paleosol types (Fig. 10). Laminated lacustrine deposits and lenticular sandbodies separate paleosols within the lower part of the Nýřany Member, while sheet like sandbodies of mostly basin-wide extent are interbeded with paleosols in the mid and upper parts of the Nýřany Member. Two paleosols were characterized in detail at the kaolin quarries.
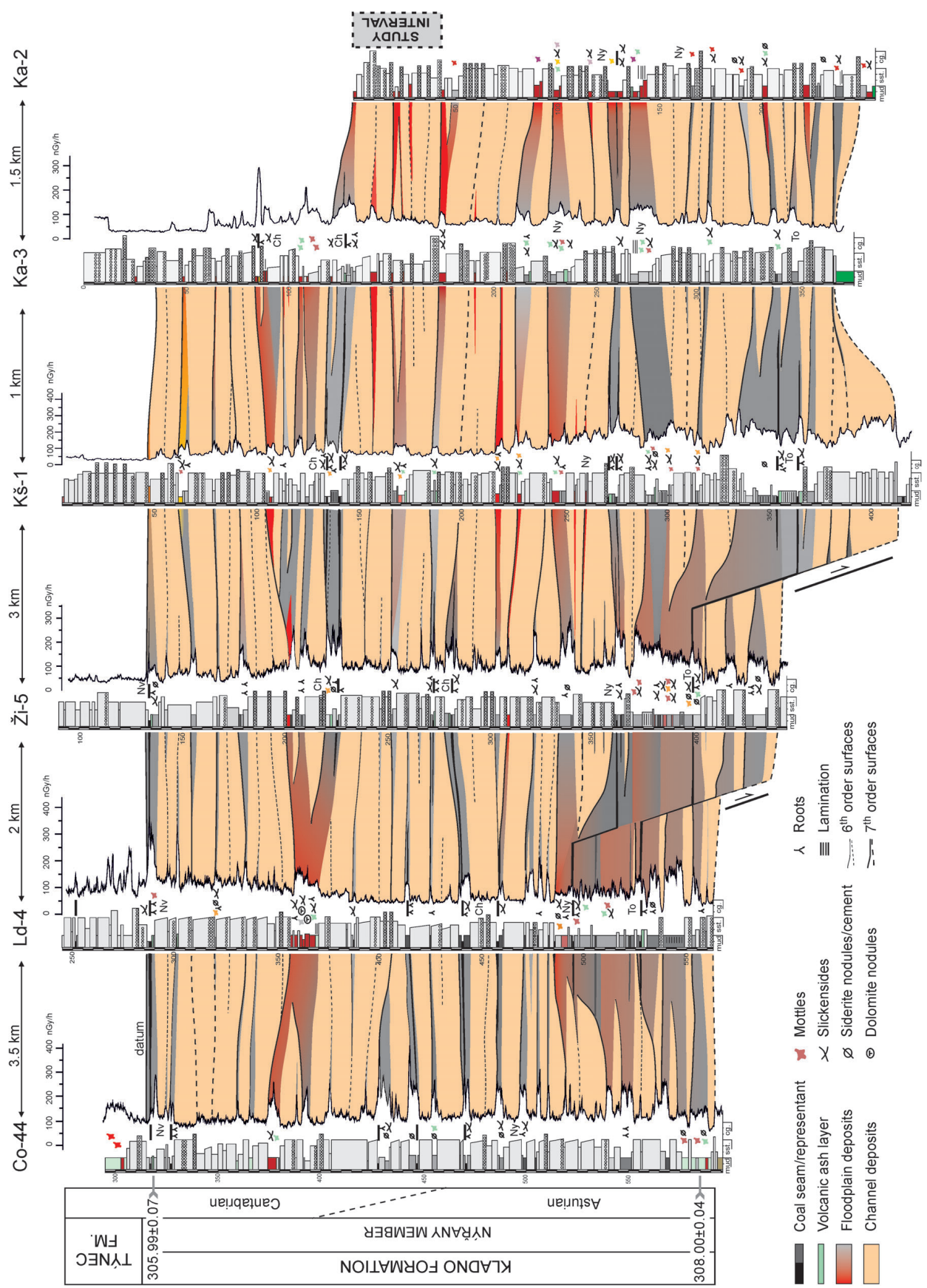
Type I paleosol

Description. – The mudstone unit at the top of the CB5 at the Kaznějov quarry contains an about 1.5 m thick type I

paleosol consisting of dominantly reddish brown mudstone that is divided into six distinctive horizons (Fig. 12), most of which are classified as Bss (slickensided B) horizons. Paleosol horizons display irregular, gradational and abrupt boundaries, except for the Bss3 horizon which is bounded by large slicken planes. The paleosol is developed on a massive variegated siltstone (C horizon), displays common slickensides, well developed fine to medium wedge shape aggregate structure and mottles and becomes clay rich up profile. The Bss1–Bss4 horizons contain large propagating slickensides and variable proportions of round, vermicular to diffuse, green, purple, orange, and yellow mottles. Some possible drab root halos are also present. The finest wedge shape agregate structure of the Bss2 horizon is accompanied by clay coatings on peds (argillans) and common fine to medium round to tubular yellow mottles (Fig. 3I). The Bss1 horizon contains few (1–3%) vermicular, yellow mottles while the uppermost Bhss horizon is rich in diffuse to vermicular light reddish brown mottles and iron-oxide concentrations.

The predominant birefringent fabrics (b-fabrics) are cross striated and parallel striated (Bullock *et al.* 1985). These b-fabrics become better developed upwards within the paleosol (Fig. 11F, G), which corresponds to macro-morphological observations and more clay rich morphologies. Potential clay lined cracks are also observed (Fig. 11E). Iron-oxide concentrations and mm-scale nodules (Fig. 11C, D) are found in the lower three Bss horizons (Bss4–Bss2), which display many diffuse vermicular light reddish brown mottles. The clay mineralogies of each horizon are very similar to one another consisting of kaolinite, illite, and subordinate mixed layer illite/smectite and accessorial goethite and hematite. There is no apparent

Figure 10. Well-log correlation panel of the Nýřany Member at the axial part at the north of the Pilsen Basin (see Fig. 1C for location) displaying cyclic patterns of alluvial deposits and lateral stability of stacked channel-belt complexes (sandbodies). Discontinuous lenticular to wedge-like sandbodies at the lower part of the Nýřany Member probably results from differential subsidence rates that fixed position of channel belts. Upwards in the stratigraphic section the sandbodies become coarser grained (increasing proportion of conglomerate), sheet-like and basin-wide with mostly planar basal surfaces. The uppermost sandbodies below the Nevřeň group of coals appear to overlie a basin-wide erosional surface reaching relief of 15 m. Group of coal seams: To – Touškov, Ny – Nýřany, Ch – Chotíkov, Nv – Nevřeň.

change in the intensity and shape of the kaolinite peak with depth; however the illite peak becomes sharper and more intense down-profile.

Interpretation. – The occurrence of well developed shrink-swell features and abundant mottling indicates that the type I paleosol is a Vertisol (Mack *et al.* 1993). The preservation of shrink-swell features suggests that the paleosol developed under conditions of repeated wetting-drying cycles in a climate characterized by seasonal precipitation (Wilding & Tessier 1988, Buol *et al.* 2003). Abundant iron-oxide concentrations, iron-oxide coated grains and cross cutting relationships indicating iron-oxide concentrations are secondary and likely formed during shallow burial. Some of the iron-oxide nodules may represent pedorelics of an older, reworked ferroan paleosol horizon. The dominance of kaolinite, subordinate illite/smectite, and the absence of carbonate nodules suggests the Vertisol formed on a well drained floodplain without prolonged periods of aridity.

Type II paleosol

Description. – The type II paleosol is observed within the mudstone unit near the base of the Horní Bříza quarry and consists of an *ca* 3.5 m thick reddish brown silty mudstone. The paleosol is divided into eight horizons that differ in colour and presence or absence of (1) slickensides, (2) wedge shape aggregate structure, and (3) mottles (Fig. 12). The paleosol horizons display clear, smooth and irregular boundaries. The lowermost *ca* 130 cm of the paleosol (2BCss, 2Bss3 and 2Bw) sharply overlies a sandstone and displays poorly developed slickensides, common coarse green mottles, iron-oxide tubules and concentrations and vertical root traces that appear to be cemented with goethite or hematite. The middle *ca* 120 cm of the paleosol (2Bss2 and 2Bss1) is finer grained and displays slickensides, well-developed fine to medium wedge shaped aggregate structure and common root halos (Fig. 3J), some of which preserve roots up to 16–20 cm long and 1 mm wide. The upper boundary with the overlying C2 horizon is abrupt and scoured. The uppermost *ca* 105 cm of this paleosol (C2, C1 and BCw) displays relict lamination, very common root halos, poorly developed slickensides, and medium wedge shape aggregate structure near the top.

Microstructures observed in the paleosol matrix include common iron oxide staining and rare oriented clay domains aligned linearly along cracks or peds (Fig. 11I). The type II paleosol lacks a well developed b-fabric and contains a higher proportion of silt compared to the type I paleosol (Fig. 11H). The clay mineral fraction is dominated by kaolinite, mixed layer illite/smectite, and illite. Illite/smectite is common in the lower part of the profile

and is quite well ordered with a low proportion of smectite layers. The uppermost horizons preserves less ordered illite/smectite with a higher proportion of smectite layers. Hematite and goethite occur in variable proportions in almost all of the samples. Chlorite appears to be absent or only accessorial in the uppermost horizons. The relative proportions of clay minerals vary throughout the profile without a clear profile scale trend. The type II paleosol, however, can be divided into lower and upper parts with the boundary at the top of 2Bss1 horizon. The upper part is dominated by kaolinite with sharp peaks and locally with elevated hematite content.

Interpretation. – The lack of a well developed soil structure including weak shrink-swell features, common redox depletions and a significant proportion of silt indicates that this paleosol is a vertic Protosol (Mack *et al.* 1993). Common laminated bedding within the upper three horizons indicates that the uppermost part of paleosol is a Protosol (Mack *et al.* 1993), and hence the type II paleosol can be interpreted as a compound paleosol sequence. Weakly developed soil structures together with a higher proportion of silt-grade material may reflect increased sediment influx to the floodplain preventing development of a mature paleosol compared to the type I paleosol.

Major element compostion of paleosols

The elemental data for matrix samples (n = 15) collected from each horizon of the type I and II paleosols are listed in Table 3; key elemental ratios (Sheldon & Tabor 2009), and weathering indices (Sheldon *et al.* 2002, CIA-K; Nordt & Driese 2010, CALMAG) are presented in Fig. 12. Calculated soil molecular weathering ratios serve as proxies for different pedogenic processes or properties and include the gleization ratio (Fe^{2+}/Fe^{3+}), clayeness (Al/Si), leaching (ΣBases/Ti), hydrolysis (ΣBases/Al), salinization (K+Na/Al), and weathering intensity (CALMAG, Nordt & Driese 2010, CIA-K, Sheldon *et al.* 2002). CIA-K values were calculated using the equation of Nesbitt & Young (1982) with K_2O removed.

Both paleosol sections display several profile-scale trends in soil molecular weathering ratios that can be associated with down-profile pedogenic trends. The type I paleosol classified as a Vertisol exhibits clear increased leaching up-profile that roughly correlates with slightly increased gleization and salinization values. The clayeyness ratio is variable with the lowest values observed in the upper part of the paleosol (Bss1–Bhss, Fig. 12). High hydrolysis ratio values within the lower to middle parts of the paleosol correspond to the lowest gleization and salinization ratios (Bss4–Bss2, Fig. 12). The type II paleosol classified as compound paleosol sequence of a vertic Protosol and Protosol displays parallel trends of hydrolysis

Table 3. Chemical composition and classification of paleosols; HB P1/4A* is lateral horizon of HB P1/4B. Abbreviations: m. silt. – muddy siltstone, s. mud. – silty mudstone.

	Sample ID	Lithology	Horizon	Paleosol classification	SiO_2	TiO_2	Al_2O_3	Fe_2O_3	FeO	MnO	MgO	CaO	Na_2O	K_2O	P_2O_5	H_2O^-	H_2O^+	CO_2	TOTAL
Type I paleosol	KA P1/6	mudstone	Bhss	Vertisol	64.85	1.22	21.54	2.72	0.05	0.01	0.26	0.15	0.12	1.89	0.04	0.53	5.81	0.30	99.49
	KA P1/5	mudstone	Bss1	Vertisol	66.85	1.11	20.94	0.88	0.02	0.01	0.24	0.16	0.11	1.85	0.03	0.51	6.32	0.29	99.32
	KA P1/4	mudstone	Bss2	Vertisol	58.42	0.94	22.81	6.63	0.09	0.01	0.23	0.15	0.10	1.68	0.06	0.61	7.29	0.37	99.39
	KA P1/3	mudstone	Bss3	Vertisol	56.44	0.87	20.66	11.47	0.05	0.01	0.23	0.13	0.10	1.43	0.10	0.64	6.97	0.35	99.45
	KA P1/2	m. silt.	Bss4	Vertisol	58.26	0.89	19.36	11.97	0.03	0.01	0.28	0.15	0.10	1.55	0.11	0.41	6.06	0.29	99.47
	KA P1/1	siltstone	C	Vertisol	62.34	1.01	23.12	2.98	0.07	0.01	0.30	0.14	0.14	2.41	0.12	0.55	6.31	0.24	99.74
Type II paleosol	HB P1/8	mudstone	BCw	Protosol	53.05	0.98	24.75	9.43	0.09	0.02	0.51	0.20	0.16	2.86	0.09	0.62	6.67	0.29	99.72
	HB P1/7	siltstone	C1	Protosol	55.23	1.01	22.99	7.88	0.11	0.02	0.56	0.17	0.16	3.21	0.12	0.72	6.75	0.39	99.32
	HB P1/6	s. mud.	C2	Protosol	39.77	0.70	15.52	34.12	0.12	0.02	0.33	0.26	0.11	2.07	0.74	0.63	4.66	0.37	99.42
	HB P1/5	mudstone	2Bss1	Vertic Protosol	55.15	1.00	19.82	12.74	0.14	0.02	0.48	0.15	0.19	3.14	0.10	0.44	5.79	0.23	99.39
	HB P1/4B	s. mud.	2Bss2	Vertic Protosol	53.05	0.88	23.05	10.46	0.19	0.01	0.58	0.22	0.22	3.72	0.27	0.58	5.94	0.30	99.47
	HB P1/4A*	s. mud.	2Bss2	Vertic Protosol	48.97	0.89	18.98	20.03	0.18	0.01	0.51	0.21	0.19	3.23	0.25	0.55	5.17	0.25	99.42
	HB P1/3	s. mud.	2Bw	Vertic Protosol	60.98	1.06	20.29	6.87	0.13	0.01	0.44	0.18	0.14	2.59	0.24	0.47	5.68	0.25	99.33
	HB P1/2	s. mud.	2Bss3	Vertic Protosol	46.60	0.83	19.11	23.59	0.15	0.01	0.39	0.23	0.12	2.25	0.12	0.55	5.39	0.24	99.58
	HB P1/1	siltstone	2BCss	Vertic Protosol	66.06	1.10	19.63	3.23	0.14	0.01	0.43	0.14	0.13	2.40	0.05	0.34	5.43	0.23	99.32

and leaching with the highest values in the lower and upper part (2BCss–2Bw, C2–BCw, Fig. 12) and the lowest values in the middle part of the compound paleosol sequence corresponding to the top of the lower vertic Protosol (2Bss2–2Bss1, Fig. 12). Salinization ratios display opposite profile-scale trend to hydrolysis. Clayeness increases systematically up-profile. The gleization ratio is generally very low and decreases up-profile.

Overall, the type II compound paleosol sequence displays lower hydrolysis and leaching ratios and higher salinization ratios than the type I paleosol, which is probably a consequence of higher sediment input (Kraus 1999) preventing long-term exposition of floodplain sediments to pedogenic processes. The higher clayeyness ratio probably reflects a relative enrichment of illite/smectite within the type II compound paleosol sequence.

Paleoprecipitation estimates

For comparative purposes, two proxies (CALMAG, Nordt & Driese 2010, CIA-K, Sheldon et al. 2002) for mean annual precipitation were utilized for the sampled paleosols. Both proxies are based upon the extent of silicate weathering with the theoretical reason being that the base forming oxides (i.e., CaO, MgO, Na_2O, and K_2O) become depleted with increased rainfall relative to Al_2O_3. The mathematical relationship between MAP and CIA-K is expressed as the following:

$$MAP \ (mm \ yr^{-1}) = 221e^{0.0197(CIA-K)}$$

where the standard error is ±181 mm yr^{-1}, and R^2 = 0.72 for the empirical relationship (Sheldon et al. 2002).

Mean annual precipitation estimates were also calculated using the relationship between CALMAG and MAP reported in Nordt & Driese (2010) for Vertisols:

$$MAP \ (mm \ yr^{-1}) = (22.69*CALMAG) – 435.8$$

where the standard error is ±108 mm yr^{-1}, and R^2 = 0.90. When applied to the same data, the CIA-K proxy results in higher MAP estimates than CALMAG in arid climates and lower estimates of MAP than CALMAG in wetter environments (CALMAG MAP > 500mm yr^{-1}; Nordt & Driese 2010). Recent comparison of the two proxies for MAP reveals that CALMAG provides more accurate MAP estimates for Vertisols compared to the CIA-K proxy (Adams et al. 2011). Accordingly, both CIA-K and CALMAG derived estimates of MAP are calculated and reported in Fig. 12, but for purposes of comparison between the both types of vertic paleosols, only CALMAG MAP estimates are used. Mean annual precipitation estimates for B horizons of the Kaznějov Vertisol using the CALMAG proxy range from 1784 to 1796 mm yr^{-1} with an average of 1791 mm yr^{-1}; alternatively, the average MAP for the B horizons of the Kaznějov Vertisol using the CIA-K proxy is 1548 mm yr^{-1} with a range of 1545 to 1551 mm yr^{-1} (Fig. 12). Using the CALMAG proxy, MAP estimates for the B horizons of the type II composite paleosol sequence at the Horní Bříza quarry range from 1750 to 1770 mm yr^{-1} with an average of 1761 mm yr^{-1}; alternatively, using the CIA-K proxy for MAP, the range of MAP for the Horní Bříza paleosol is 1522 to 1543 mm yr^{-1}, with an average 1532 mm yr^{-1} (Fig. 12). Considering the uncertainty associated with the

CALMAG MAP relationship (±108 mm yr^{-1}), the MAP estimates between the type I and type II paleosols are statistically indistinguishable, suggesting the both sets of paleosols are recording similar environmental conditions (MAP *ca* 1776 mm yr^{-1}) during active pedogenesis.

Discussion

Autogenic controls on alluvial architecture

Analysis of the Nýřany Member fluvial strata exposed at the Kaznějov and Horní Bříza quarries at the northern part of the Pilsen Basin indicates that rivers were composed of at least one trunk channel that was associated with several second order channels of low to intermediate sinuosity confirming previous interpretations (Opluštil *et al.* 2005). The paleocurrent directions are dominantly south to south-westward suggesting an axial drainage pattern, which is consistent with previous research (Pešek 1968). The observed scale of the architectural components and facies composition display a strong correlation with the architectural model of a deep perennial gravel-bed braided river of Donjek type (Miall 1996) characterized by several active higher sinuosity channels divided by large braid bars growing laterally, downstream and upstream. Modes of paleocurrent dispersion within and between channel belts and common lateral accretion implies a rather low gradient topography and rather tributary pattern of this axial fluvial system.

The morphology of the channel belt formed during large magnitude floods as a result of avulsion and incision of channels. Channels that were established during maximum bankfull discharge were further modified and gradually filled by passing channel-bar systems. The stacking pattern of channel-bar systems within a channel belt was mainly controlled by intra-channel belt processes including channel migration and bar accretion, seasonal fluctuation and local, anabranch avulsion. Local avulsion is evidenced by incision surfaces and mudstone rip-up clasts and results from locally increased channel aggradation rates (Leddy *et al.* 1993, Heller & Paola 1996). The rest of the abandoned channel still represents a topographic low providing a favourable pathway for the new channel to reoccupy the previous channel downstream resulting in channel clusters. Under low mean aggradation rates (*ca* 0.15 mm yr^{-1}) local avulsion generates stacked multistorey channel belts dominated by channel and bar deposits (Heller & Paola 1996, Mohrig *et al.* 2000, Chamberlin & Hajek 2015). Under such conditions, even low to moderate rates of lateral migration of channels would cause superposition of channel bars and fills before the channel-belt is abandoned, resulting in a multistorey character of the channel belt (Bridge & Mackey 1993a).

At the channel belt scale, the most likely process controlling the alluvial architecture is regional avulsion (Heller & Paola 1996). A significant period of time between channel belt abandonment and reoccupation allows floodplain deposits to aggrade to a significant thickness. Erosive processes due to re-establishment of the new active channel belt remove much or all of the floodplain deposits, resulting in preservation of the underlying bar deposits (McLaurin & Steel 2007). Hajek *et al.* (2010) observed internal self-organization of fluvial systems leading to non-random channel clustering; this suggests that river avulsion is a structured process on basin filling time scales. In the absence of changing external controls channel belt clustering could be driven by long-time scale organization in river avulsion and migration around a basin. This type of autogenic avulsion clustering suggests a bimodal distribution of avulsion lengths where commonly channels do not move very far from one another but occasionally large-scale avulsions move the system to a new location within a basin. This channel belt clustering may reflect compensational filling within an alluvial basin and result in a channel belt controlled by regional-scale avulsion containing multiple channels under the influence of local avulsion (Hajek *et al.* 2010). This supports the idea that channel belt scale bodies are a result of autogenic processes.

Allogenic controls on basin fill architecture

Stacked channel-belt complexes represent the most prominent architectural element on the basin fill scale. There are about 14 to 22 stacked channel-belt complexes within the Nýřany Member at the northern part of the Pilsen Basin that form either sheet like units extending basin-wide or lenticular units that wedge out to laterally equivalent interfluve paleosols (Fig. 10). The geometry of the stacked channel-belt complexes in the axial cross section varies vertically likely reflecting activity on the NW oriented faults, a conjungate system to the N–S trending central trench (Pešek 1968, Pašek & Urban 1990). Lenticular sandbodies observed at several stratigraphic levels may reflect periods of higher diferential subsidence rate, especially during deposition of the lower part of the Nýřany Member (Pešek 1994).

The processes controlling cyclicity at the scale of stacked channel-belt complexes are questionable with minor evidence to support an allocyclic effect on architectural style. Mature paleosols developed in floodplain mudstones above stacked channel-belt complexes indicate prolonged periods of depositional quiescence across a large area of the basin. The preservation of thick, basin-wide floodplain mudstone in such a dynamic fluvial environment implies an even higher original thickness likely due to prominent aggradational events. These characteristics may signify ac-
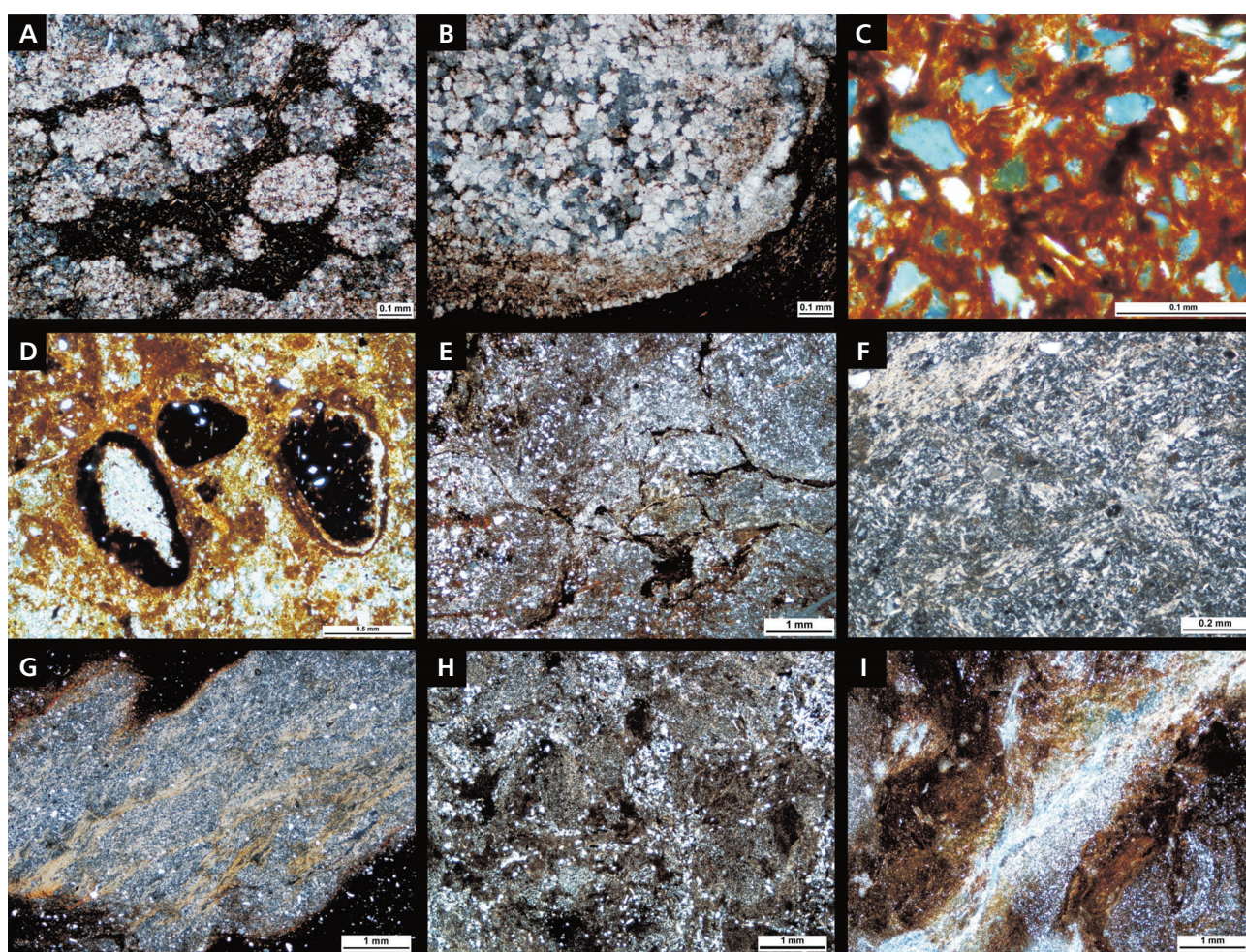
Figure 11. Microphotographs of paleosol matrix. • A – fine dolomicrite nodules dispersed in clayey paleosol matrix stained with iron-oxides (LD-4 well core, 365.9 m, Fig. 10). • B – rhomboedral crystallites in the center and fine micrite at the edge of a dolomite nodule (LD-4 borehole core, 365.9 m, Fig. 10). • C – iron-oxides concentrations coating and replacing quartz grains (Bss4, type I paleosol). • D – sharply bounded mm-scale iron-oxide nodules or possible pedorelics in clayey matrix stained with iron-oxides (Bss3, type I paleosol). • E – potential clays lining cracks near the center of photo accompanied by iron-oxides (Bss2, type I paleosol). • F – oriented clays and minimal iron-oxides staining within the upper horizon of the type I paleosol (Bss1). • G – well developed oriented clay fabrics in the uppermost horizon of the type I paleosol (Bhss). • H – mottling, iron-oxide staining and concentrations and increased silt fraction typical for the type II paleosol (2Bw). • I – linear arrangement of redox depletion developing around original roots (2Bss2, type II paleosol).

commodation creation/destruction related to changes in stream equilibrium profile manifested by water-table fluctuations on the scale of the stacked channel-belt complexes. Finer grain size and smaller dimensions of channels in the floodplain units suggest a decrese in sediment supply and flood discharge, which would be consistent with a decrease in seasonality and a more even MAP distribution reflecting a stabilized climate resulting in a higher water-table level. Climatic variation commonly drives incision and aggradation cycles in modern valleys and is an attractive explanation for the 7th order surfaces bounding stacked channel-belt complexes (Holbrook 2001). Cycles of valley incision and filling are argued to reflect regional variations in discharge regimes and sediment supply within Quaternary (Blum & Tornqvist 2000, Leeder *et al.* 1998).

Globally synchronous changes in sedimentation and erosion rates observed in the Quaternary has been explained to be driven by climate that affect erosion mainly by the transition from a period of climate stability, in which landscapes had attained equilibrium configurations, to a time of frequent and abrupt changes in temperature, precipitation and vegetation, which prevented fluvial and glacial systems from establishing equilibrium states (Peizhen *et al.* 2001).

The mean time interval required for the formation of stacked channel-belt complex may be roughly estimated by using the number of cycles between dated layers. According to well-log records and correlations, there are between 14 to 22 stacked channel belt complexes within the *ca* 2 m.y. time interval of the Nýřany Member in the Pilsen

Basin (Opluštil *et al.* 2016) indicating that the maximum average duration of each cycle should be less than *ca* 140 k.y. This conforms to the eccentricity cycle of Earth's orbit that was inferred to control low-latitude precipitation in late Paleozoic via amplification of precession-driven changes in insolation that increased low-latitude precipitation variability during periods of high eccentricity. When eccentricity was low, the amplification of precessionally driven insolation fluctuations was reduced, which promoted less variable low-latitude precipitation and landscape stabilization (Horton *et al.* 2012).

Paleoweathering and paleoclimate

The alluvial strata of the Nýřany Member display evidence of a deep perennial gravel-bed braided river system that contained several at least 147–306 m wide channels of mean flow depth 4.7–7 m transporting large amount of coarse clastic material and undergoing prominent discharge fluctuations. High sediment supply allowing for rapid channel aggradation together with common discharge fluctuations promoted increased avulsion frequency that generated multistory sandbodies with rarely preserved floodplain mudstone. Intervals of thalweg fill and barform dominated zones are indicative of increased sediment yield and represent periods of climate instability with strongly seasonal rainfall and less dense vegetation cover, leading to high erosion rates and runoff during intense rainfall events (Hooke 2000). The chemically mature siliciclastic material dominated by quartz and other resistant rock fragments likely resulted from a combination of (1) intense chemical weathering during prolonged transport and (2) multiple redepositions before final sedimentation. Sandstones contain up to 15% kaolinite formed by leaching of feldspars that likely initiated in the source area and continued during transport and final deposition in alluvium; this is also indicated by buried kaolin-rich sections overlain by kaolinite-depleted alluvial deposits (Kužvart *et al.* 1975).
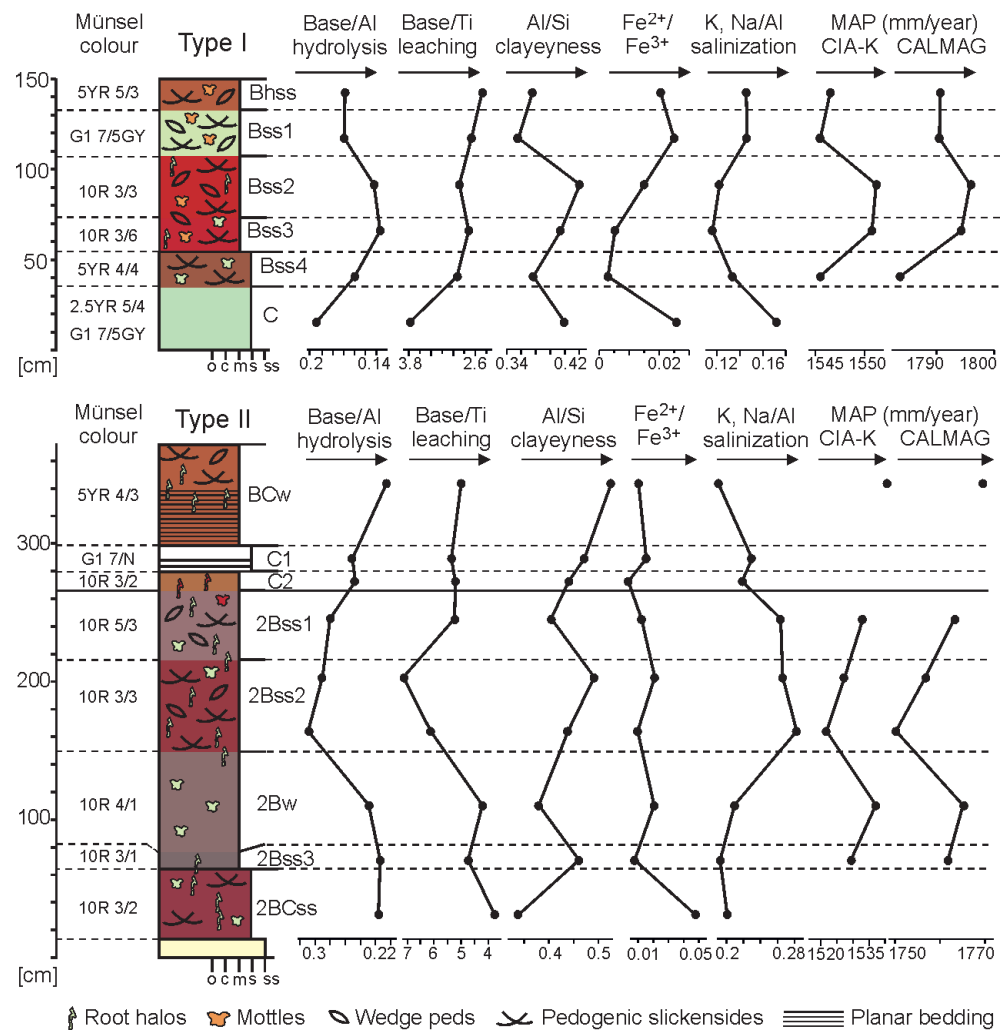
Mudstone-dominated floodplains separating sandbodies represent periods of stabilized climate associated with high water-table level generating elevated aggradational rates. Rarely observed relatively small (80–200 m wide), shallow (*ca* 3 m deep) and finer-grained channel bodies support reduced discharge fluctuation and suppressed sediment supply during climate stabilization that would also reduce avulsion frequency leaving the active channel belt in a stable position for a significant period of time. Kaolinite rich paleosols formed under a generally high, but fluctuating, water table that gave rise to a dense and diversified vegetation cover that further stabilized the landscape (Bashforth *et al.* 2011). Based upon well-log correlations the vertic paleosols indicative of fluctuating

water table grade laterally to water-logged paleosols, including coals, which are characteristic of a high and stable water-table. These lateral (spatial) variations of paleosol types may reflect alluvial plain topography. Protosols are interpreted to have formed on unstable landscapes, such as a proximal alluvial plain close to channel margins, which resulted in increased and intermittent clastic input (*e.g.*, Marriott & Wright 1993, Kraus 1997). Alternatively, Vertisols developed on stable interfluvial areas of well-drained floodplains with a fluctuating water-table and/or seasonal precipitation.

Kaolinite is typically formed by weathering of aluminosilicates under acidic, warm, humid conditions in well-drained and highly weathered soils characterized by long periods of leaching (Dixon & Skinner 1992, Wilson 1999). In modern Vertisols, the development of wedge-shaped aggregate structure and slickensides typically results from shrink-swell processes associated with expandable 2:1 phyllosilicates (*e.g.*, smectite) in climates that experience seasonal precipitation and/or episodic changes in water-table position (Yaalon & Kalmar 1978, Driese *et al.* 2005). Akin to the Pennsylvanian record in the Illinois Basin (Rosenau *et al.* 2013), paleosols documented herein differ from modern Vertisols in their lack of smectite and subordinate presence of interstratified illite-rich illite/smectite in < 2 μm fraction. This could be the result of low-temperature illitization of smectite to I/S in the pedogenic environment during fluctuating redox conditions as a result of seasonal wetting and drying cycles (*e.g.*, Watts 1980, Robinson & Wright 1987, Deconinck *et al.* 1988, Huggett & Cuadros 2003, Rosenau *et al.* 2013).

There are two possible modes of preservation of silicified wood (mostly *Dadoxylon* sp., corresponding to a fossil Cordaitalean tree trunks) in the alluvial strata of the Nýřany Member including parts of tree trunks transported as wooden material and deposited either in relatively fine-grained facies at the upper bar deposits or in channel thalwegs where *in situ* silicification took place. Silicified tree trunk cobbles with rounded smooth faces (Fig. 4) suggest they may have been silicified prior to transport and deposition in river thalwegs. The depth of erosion during incision of channel belts (< 8 m) implies that tree trunk silicification should have occurred in the shallow subsurface. As suggested by many authors (*e.g.*, Skoček 1970, Weibel 1996, Nowak *et al.* 2005, Matysová *et al.* 2010) feldspars in arkoses are the most likely silica source for tree trunk silicification. As such, it is interpreted that leaching of feldspars, kaolinite formation and tree trunk silicification are related processes operating close to the depositional surface, likely during pedogenesis after regional avulsion. Paleoprecipitation estimates of 1800 mm yr^{-1} and seasonal water-table fluctuations under warm climate is required for silicification of tree trunks in river alluvium.

Figure 12. The two paleosol sections plotted with key elemental ratios, weathering indices and inferred paleoprecipitation.

Root halos Mottles Wedge peds Pedogenic slickensides Planar bedding

Conclusions

Strata of the Nýřany Member at the northern part of the Pilsen Basin were deposited in a perennial gravel-bed braided fluvial system that contained several active channels of low to intermediate sinuosity. Channels with a mean flow depth of 4–7 m underwent strong discharge fluctuations reaching maximum bankfull flow depth of about 15 m with active channel belt width about 2 km.

The three main architectural components identified are: (1) sheet-like and lenticular conglomerates of thalweg fills, (2) inclined gravel-sand and sandy strata of barforms and (3) mudstone units representing floodplains and abandoned channel fills. These architectural elements stack to form the three-fold cyclic hierarchy represented by channel-bar systems (3–10 m thick), channel belts (4–15 m thick) and stacked channel-belt complexes (10–35 m thick).

The smallest scale cycles of channel-bar systems were generated by channel migration. Low mean aggradation rates and frequent channel migration preserving the topo-graphically lowest parts of the passing channel-bar systems resulted in a succession of superimposed thalweg fills with poorly or unpreserved bars, termed composite thalweg units. Local avulsion and channel migration controlled the stacking pattern of channel-bar systems in the channel belt. Planar erosional surfaces separating vertically stacked channel belts resulted from regional avulsions.

Large-scale cycles of stacked channel belt complexes (sandbodies) are composed of several superimposed channel belts capped by laterally extensive floodplains that display evidence of decreased seasonality and precipitation of *ca* 1800 mm yr^{-1}. Such conditions would be characteristic for a stable climate of the Pennsylvanian paleotropics and would promote a rise of the water-table resulting in increasing accommodation. At the basin marginal setting, periods of stable climate were characterized by a high, but fluctuating, water-table accompanied by extensive leaching of feldspars, Vertisol formation, kaolinite precipitation and tree trunk silicification close to the depositional surface. The average time interval required for the formation of stacked channel belt complexes is less than *ca* 140 k.y.,

implying that the eccentricity cycle of Earth's orbit could be a driving force controlling climate stability in the interior basins of Pennsylvanian paleotropics.

Additional correlations of the Nýřany Member fluvial strata in the Pilsen Basin and adjacent Kladno-Rakovník Basin are needed to constrain the geometry of these large-scale cycles and to better understand the allogenic processes that controlled the basin fill architecture.

Acknowledgments

References

Adams, J.S., Kraus, M.J. & Wing, S.L. 2011. Evaluating the use of weathering indices for determining mean annual precipitation in the ancient stratigraphic record. *Palaeogeography, Palaeoclimatology, Palaeoecology 309*, 358–366. DOI 10.1016/j.palaeo.2011.07.004

Allen, J.R.L. 1983. Studies in fluviatile sedimentation: bars, bar-complexes and sandstone sheets (low-sinuosity braided streams) in the brownstones (L. Devonian), Welsh Borders. *Sedimentary Geology 22*, 237–293. DOI 10.1016/0037-0738(83)90076-3

Allen, J.P. & Fielding, C.R. 2007. Sedimentology and stratigraphic architecture of the Late Permian Betts Creek Beds, Queensland, Australia. *Sedimentary Geology 202*, 5–34. DOI 10.1016/j.sedgeo.2006.12.010

Allen, J.P., Fielding, C.R., Gibling, M.R. & Rygel, M.C. 2011. Fluvial response to paleo-equatorial climate fluctuations during the late Paleozoic ice age. *Geological Society of America Bulletin 123(7–8)*, 1524–1538. DOI 10.1130/B30314.1

Ashmore, P.E. 1993. Anabranch confluences kinetics and sedimentation processes in gravel-braided streams, 129–146. *In* Best, J.L. & Bristow, C.S. (eds) *Braided Rivers.* Special Publication 75, Geological Society Publishing House, Bath.

Atchley, S.C., Nordt, L.C. & Dworkin, S.I. 2004. Eustatic control on alluvial sequence stratigraphy: a possible example from the Cretaceous-Tertiary transition of the Tornillo Basin, Big Bend National Park, west Texas, U.S.A. *Journal of Sedimentary Research 74*, 391–404. DOI 10.1306/102203740391

Bashforth, A.R., Drábková, J., Opluštil, S., Gibling, M.R. & Falcon-Lang, H.J. 2011. Landscape gradients and patchiness in riparian vegetation on a middle Pennsylvanian braided-river plain prone to flood disturbance (Nýřany Member, Central and Western Bohemian Basin, Czech Republic). *Review of Paleobotany and Palynology 163*, 153–189. DOI 10.1016/j.revpalbo.2010.10.001

Best, J.L., Ashworth, P.J., Bristow, C.S. & Roden, J. 2003. Three-dimensional sedimentary architecture of a large, mid-channel sand braid bar, Jamuna River, Bangladesh. *Journal of Sedimentary Research 76(5)*, 731–770. DOI 10.1306/010603730516

Birgenheier, L.P., Fielding, C.R., Rygel, M.C., Frank, T.D. & Roberts, J. 2009. Evidence for dynamic climate change on sub 10^6-year scales from the late Paleozoic glacial record, Tamworth Belt, New South Wales, Australia. *Journal of Sedimentary Research 79(2)*, 56–82. DOI 10.2110/jsr.2009.013

Blum, M.D. & Tornqvist, T.E. 2000. Fluvial response to climate and sea-level: a review and look forward. *Sedimentology 47*, 1–48. DOI 10.1046/j.1365-3091.2000.00008.x

Bridge, J.S. 1993a. Description and interpretation of fluvial deposits. *Sedimentology 40*, 801–810. DOI 10.1111/j.1365-3091.1993.tb01361.x

Bridge, J.S. 1993b. The interaction between channel geometry, water flow, sediment transport, erosion and deposition in braided rivers, 13–71. *In* Best, J.L. & Bristow, C.S. (eds) *Braided Rivers.* Special Publication 75, Geological Society Publishing House, Bath.

Bridge, J.S. & Leeder, M.R. 1979. A simulation model of alluvial stratigraphy. *Sedimentology 26*, 617–644. DOI 10.1111/j.1365-3091.1979.tb00935.x

Bridge, J.S. & Mackey, S.D. 1993a. A revised alluvial stratigraphy model, 319–337. *In* Marzo, M. & Puigdefabregas (eds) *Alluvial sedimentation. International Association of Sedimentologists, Special Publication 17.*

Bridge, J.S. & Mackey, S.D. 1993b. A theoretical study of fluvial sandstone body dimensions, 213–236. *In* Flint, S.S. & Bryant, I.D. (eds) *Geological modeling of hydrocarbon reservoirs. International Association of Sedimentologists, Special Publication 15.*

Bridge, J.S. & Tye, R.S. 2000. Interpreting the dimensions of ancient fluvial channel bars, channels and channel belts from wireline logs and cores. *Bulletin of American Association of Petroleum Geologists 84(8)*, 1205–1228.

Bristow, C.S. & Best, J.L. 1993. Braided rivers: perspective and problems, 1–11. *In* Best, J.L. & Bristow, C.S. (eds) *Braided Rivers.* Special Publication 75, Geological Society Publishing House, Bath.

Bullock, P., Federoff, N., Jongerius, A., Stoops, G. & Tursina, T. 1985. *Handbook for Soil Thin Section Description.* 152 pp. Waine Research Publications, Wolverhampton.

Buol, S.W., Southard, R.J., Graham, R.C. & McDaniel, P.A. 2003. *Soil Genesis and Classification. Fifth edition.* 494 pp. Iowa State University Press, Ames.

Chamberlin, E.P. & Hajek, E.A. 2015. Interpreting paleo-avul-

sion dynamics from multistory sand bodies. *Journal of Sedimentary Research 85*, 82–94. DOI 10.2110/jsr.2015.09

CLEAL, C.J., JAMES, R.M. & ZODROW, E.L. 1999. Variation in stomatal density in the Late Carboniferous gymnosperm frond *Neuropteris ovata. Palaios 14*, 180–185.
DOI 10.2307/3515373

CLEAL, C.J. & THOMAS, B.A. 2005. Palaeozoic tropical rainforests and their effect on global climates: is the past the key to the present? *Geobiology 3*, 13–31.
DOI 10.1111/j.1472-4669.2005.00043.x

DECONINCK, J.F., STRASSER, A. & DEBRABANT, P. 1988. Formation of illitic minerals at surface temperatures in Purbeckian sediments (lower Berrasian, Swiss and French Jura). *Clay Minerals 23*, 91–104. DOI 10.1180/claymin.1988.023.1.09

DIMICHELE, W.A., PFEFFERKORN, H.W. & GASTALDO, R.A. 2001. Response of Late Carboniferous and Early Permian plant communities to climate change. *Annual Review of Earth and Planetary Sciences 29*, 461–487.
DOI 10.1146/annurev.earth.29.1.461

DIXON, J.B. & SKINNER, H.C.W. 1992. Manganese minerals in surface environments, 31–50. *In* SKINNER, H.C.W. & FITZPATRICK, R.W. (eds) *Biomineralization Processes of Iron and Manganese*. Catena-Verlag, Cremlingen-Destedt.

DRIESE, S.G., NORDT, L.C., LYNN, W., STILES, C.A., MORA, C.I. & WILDING, L.P. 2005. Distinguishing climate in the soil record using chemical trends in a Vertisol climosequence from the Texas Coastal Prairie, and application to interpreting Paleozoic paleosols in the Appalachian Basin, U.S.A. *Journal of Sedimentary Research 75(3)*, 340–353.
DOI 10.2110/jsr.2005.027

ELZNIC, A., CHÁB, J. & PEŠEK, J. 1974. A graben structure striking north-northeast-south-southwest in the Plzeň and the Žihle basins. *Folia Musei rerum naturalium Bohemiae occidentalis, Geologica 4*.

ETHERIDGE, F.G. & SCHUMM, S.A. 1978. Reconstructing palaeochannel morphologic and flow characteristics: methodology, limitations and assessment, 703–721. *In* MIALL, A.D. (ed.) *Fluvial sedimentology. Canadian Society of Petroleum Geologists Memoir 5*.

FELDMAN, H.R., FRANSEEN, E.K., JOECKEL, R.M. & HECKEL, P.H. 2005. Impact of longer-term modest climate shifts on architecture of high-frequency sequences (cyclothems), Pennsylvanian of midcontinent U.S.A. *Journal of Sedimentary Research 75(3)*, 350–368. DOI 10.2110/jsr.2005.028

FERGUSON, R.I. 1993. Understanding braiding processes in gravel bed rivers: progress and unsolved problems, 73–87. *In* BEST, J.L. & BRISTOW, C.S. (eds) *Braided Rivers.* Special Publication 75, Geological Society Publishing House, Bath.

FRIEND, P.F. 1983. Towards the field classification of alluvial architecture or sequence, 531–542. *In* COLLINSON, J.D. & LEWIN, J. (eds) *Modern and ancient fluvial systems. International Association of Sedimentologists, Special Publication 6*.

FRIEND, P.F., SLATER, M.J. & WILLIAMS, R.C. 1979. Vertical and lateral building of river sandstone bodies, Ebro Basin, Spain. *Journal of Geological Sociaety of London 136*, 39–46.
DOI 10.1144/gsjgs.136.1.0039

GHOSH, P. 2000. Estimation of channel sinuosity from paleocurrent data: a method using fractal geometry. *Journal of Sedimentary Research 70(3)*, 449–455.
DOI 10.1306/2DC4091D-0E47-11D7-8643000102C1865D

GIBLING, M.R. 2006. Width and thickness of fluvial channel bodies and valley fills in the geological record: a literature compilation and classification. *Journal of Sedimentary Research 76(5)*, 731–770. DOI 10.2110/jsr.2006.060

GIBLING, M.R. & BIRD, J.D. 1994. Late Carboniferous cyclothems and alluvial paleovalleys in the Sydney Basin, Nova Scotia. *Geological Society of America Bulletin 106(1)*, 105–117.
DOI 10.1130/0016-7606(1994)106<0105:LCCAAP>2.3.CO;2

GODIN, P. 1991. Fining-upwards cycles in the sandy-braided river deposits of the Westwater Canyon Member (Upper Jurassic), Morrison Formation, New Mexico. *Sedimentary Geology 70*, 61–82. DOI 10.1016/0037-0738(91)90066-M

GULBRANSON, E.L., MONTANEZ, I.P., TABOR, N.J. & LIMARINO, O.C. 2015. Late Pennsylvanian aridification on the southwestern margin of Gondwana (Paganzo Basin, NW Argentina): A regional expression of a global climate pertubation. *Palaeogeography, Palaeoclimatology, Palaeoecology 417(1)*, 220–235. DOI 10.1016/j.palaeo.2014.10.029

GUSTAVSON, T.C. 1978. Bed forms and stratification types of modern gavel meander lobes, Nueces River, Texas. *Sedimentology 25*, 401–426.
DOI 10.1111/j.1365-3091.1978.tb00319.x

HAJEK, E.A., HELLER, P.L. & SHEETS, B.A. 2010. Significance of channel-belt clustering in alluvial basins. *Geology 38(6)*, 535–538. DOI 10.1130/G30783.1

HAVLENA, V. 1977. Late Paleozoic basins of the Bohemian Massif, 173–182. *In* HOLUB, W.M. & WAGNER, R.H. (eds) *Symposium on Carboniferous Stratigraphy*. Ústřední ústav geologický, Prague.

HAVLENA, V. & PEŠEK, J. 1980. Stratigrafie, paleogeografie a základní strukturní členění limnického permokarbonu Čech a Moravy. *Sborník Příroda 34*. Pilsen. [in Czech]

HELLER, P.L. & PAOLA, C. 1996. Downstream changes in alluvial architecture: an exploration of controls on channel-stacking patterns. *Journal of Sedimentary Research 66(2)*, 297–306.

HOLBROOK, J. 2001. Origin, genetic interrelationships, and stratigraphy over the continuum of fluvial channel-form bounding surfaces: an illustration from middle Cretaceous strata, southeastern Colorado. *Sedimentary Geology 144*, 179–222.
DOI 10.1016/S0037-0738(01)00118-X

HOOKE, R. LEB. 2000. Toward a uniform theory of clastic sediment yield in fluvial systems. *Geological Society of America Bulletin 112(12)*, 1778–1786.
DOI 10.1130/0016-7606(2000)112<1778:TAUTOC>2.0.CO;2

HORTON, D.E., POULSEN, C.J., MONTAÑEZ, I.P. & DIMICHELE, W.A. 2012. Eccentricity-paced late Paleozoic climate change. *Palaeogeography, Palaeoclimatology, Palaeoecology 331–332*, 150–161. DOI 10.1016/j.palaeo.2012.03.014

HUGGETT, J.M. & CUADROS, J. 2003. Low-temperature illitization of smectite in the late Eocene and early Oligocene of the Isle of Wight (Hampshire Basin), U.K. *American Mineralogist 90*, 1192–1202. DOI 10.2138/am.2005.1674

JOHNSON, W.M. & MAXWELL, J.A. 1981. *Rock and Mineral Analysis*. 489 pp. Wiley, New York.

KRAUS, M.J. 1997. Lower Eocene alluvial Paleosols: pedogenic development, stratigraphic relationships, and paleosol/landscape associations. *Palaeogeography, Palaeoclimatology, Palaeoecology 129*, 387–406.
DOI 10.1016/S0031-0182(96)00056-9

KRAUS, M.J. 1999. Paleosols in clastic sedimentary rocks: their geologic significance. *Earth-Science Reviews 47*, 41–70.
DOI 10.1016/S0012-8252(99)00026-4

KHADKIKAR, A.S. 1999. Trough cross-bedded conglomerate facies. *Sedimentary Geology 128(1–2)*, 39–49.
DOI 10.1016/S0037-0738(99)00060-3

KRS, M. & PRUNER, P. 1995. Palaeomagnetism and palaeogeography of the Variscan formations of the Bohemian Massif, comparison with other European regions. *Journal of Czech Geological Society 40*, 3–46.

KUŽVART, M., NEUŽIL, J., PEŠEK, J. & ŠINDELÁŘ, J. 1975. Vznik a stáří ložisek kaolínu v plzeňské pánvi. *Sborník geologických věd 17, Ložisková geologie*, 125–241. [in Czech]

LECLAIR, S. & BRIDGE, J.S. 2001. Quantitative interpretation of sedimentary structures formed by rived dunes. *Journal of Sedimentary Research 71(5)*, 713–716.
DOI 10.1306/2DC40962-0E47-11D7-8643000102C1865D

LEDDY, J.O., ASHWORTH, P.J. & BEST, J.L 1993. Mechanisms of anabranch avulsion within gravel-bed braided rivers: observations from a scaled physical model, 119–127. *In* BEST, J.L. & BRISTOW, C.S. (eds) *Braided Rivers.* Special Publication 75, Geological Society Publishing House, Bath.

LEEDER, M.R., HARRIS, T. & KIRBY, M.J. 1998. Sediment supply and climate change: implications for basin stratigraphy. *Basin Research 10*, 7–18.
DOI 10.1046/j.1365-2117.1998.00054.x

LELEU, S., HARTLEY, A.J. & WILLIAMS, B.P.J. 2009. Large-scale alluvial architecture and correlation in a Triassic pebbly braided river system, lower Wolfville Formation (Fundy Basin, Nova Scotia, Canada). *Journal of Sedimentary Research 79(5)*, 265–286. DOI 10.2110/jsr.2009.034

LEWIN, J. & MACKLIN, M.G. 2003. Preservation potential for Late Quarternary river alluvium. *Journal of Quarternary Science 18*, 107–120. DOI 10.1002/jqs.738

LOJKA, R., SÝKOROVÁ, I., LAURIN, J., MATYSOVÁ, P. & GRYGAR, T.M. 2010. Lacustrine couplet-lamination: evidence for Late Pennsylvanian seasonality in central equatorial Pangaea (Stephanian B, Mšec Member, Central and Western Bohemian basins). *Bulletin of Geosciences 85(4)*, 709–734.
DOI 10.3140/bull.geosci.1210

LÓPEZ-GÓMEZ, J. & ARCHE, A. 1993. Architecture of the Cañiyar fluvial sheet sandstones, Early Triassic, Iberian Ranges, Eastern Spain, 363–381. *In* MARZO, M. & PUIGDEFABREGAS, C. (eds) *Alluvial Sedimentation. International Association of Sedimentologists, Special Publication 17.*

LUNT, I.A, BRIDGE, J.S. & TYE, R.S. 2004. A quantitative, three-dimensional depositional model of gravelly braided rivers. *Sedimentology 51*, 377–414.
DOI 10.1111/j.1365-3091.2004.00627.x

MACK, G.H., JAMES, W.C. & MONGER, H.C. 1993. Classification of paleosols. *Geological Society of America Bulletin 105*, 129–136.
DOI 10.1130/0016-7606(1993)105<0129:COP>2.3.CO;2

MARRIOTT, S.B. & WRIGHT, V.P. 1993. Paleosols as indicators of geomorphic stability in two Old Red Sandstone alluvial suites, South Wales. *Journal of Geological Society of London 150*, 1109–1120. DOI 10.1144/gsjgs.150.6.1109

MATYSOVÁ, P., RÖSSLER, R., GÖTZE, J., LEICHMANN, J., FORBES, G., TAYLOR, E.R., SAKALA, J. & GRYGAR, T. 2010. Alluvial and volcanic pathways to silicified plant stems (Upper Carboniferous–Triassic) and their taphonomic and palaeoenvironmental meaning. *Palaeogeography, Palaeoclimatology, Palaeoecology 292*, 127–143. DOI 10.1016/j.palaeo.2010.03.036

McLAURIN, B.T. & STEEL, R.J. 2007. Architecture and origin of an amalgamated fluvial sheet sand, lower Castlegate Formation, Book Cliffs, Utah. *Sedimentary Geology 197*, 291–311.
DOI 10.1016/j.sedgeo.2006.10.005

MIALL, A.D. 1980. Cyclicity and the facies model concept in fluvial deposits. *Bulletin of Canadian Petroleum Geology 28*, 59–80.

MIALL, A.D. 1988. Architectural elements and bounding surfaces in fluvial depostis: Anatomy of Kayenta Formation (lower Jurrasic), southwest Colorado. *Sedimentary Geology 55*, 233–262. DOI 10.1016/0037-0738(88)90133-9

MIALL, A.D. 1996. *The geology of fluvial deposits.* 582 pp. Springer-Verlag, New York.

MOHRIG, D., HELLER, P.L., PAOLA, C. & LYONS, W.J. 2000. Interpreting avulsion process from ancient alluvial sequences: Gaudalope-Matarranya system (northern Spain) and Wasatch Formation (western Colorado). *Geological Society of America Bulletin 112*, 1787–1803.
DOI 10.1130/0016-7606(2000)112<1787:IAPFAA>2.0.CO;2

NEMEC, W. & POSTMA, G. 1993. Quarternary alluvial fans in southwestern Crete: sedimentation processes and geomorphic evolution, 235–276. *In* MARZO, M. & PUIGDEFABREGAS, C. (eds) *Alluvial Sedimentation. International Association of Sedimentologists, Special Publication 17.*

NĚMEJC, F. 1953. *Úvod do floristické stratigrafie kamenouhelných oblastí ČSR.* 173 pp. Academia, Praha.

NESBITT, H.W. & YOUNG, G.M. 1982. Early Proterozoic climates and plate motions inferred from major element chemistry of lutites. *Nature 299*, 715–717. DOI 10.1038/299715a0

NORDT, L.C. & DRIESE, S.D. 2010. New weathering index improves paleorainfall estimates from Vertisols. *Geology 38*, 407–410. DOI 10.1130/G30689.1

NOWAK, J., FLOREK, M., KWIATEK, W., LEKKI, J., CHEVALIER, P., ZIĘBA, E., MESTRES, N., DUTKIEWICZ, E.M. & KUCZUMOW, A. 2005. Composite structure of wood cells in petrified wood. *Materials Science and Engineering C 25*, 119–130.
DOI 10.1016/j.msec.2005.01.018

OLSEN, T., STEEL, R., HØGSETH, K., SKAR, T. & RØE, S.L. 1995. Sequential architecture in a fluvial succession: sequence stratigraphy in the Upper Cretaceous Mesaverde Group, Price Canyon, Utah. *Journal of Sedimentary Research B 65(2)*, 265–280.
DOI 10.1306/D426822A-2B26-11D7-8648000102C1865D

OPLUŠTIL, S. 2005. Evolution of the Middle Westphalian river valley drainage system in central Bohemia (Czech Republic) and its palaeogeographic implication. *Palaeogeography, Palaeoclimatology, Palaeoecology 222(3–4)*, 223–258. DOI 10.1016/j.palaeo.2005.03.016

OPLUŠTIL, S., MARTÍNEK, K. & TASÁRYOVÁ, Z. 2005. Facies and architectural analysis of fluvial deposits of the Nýřany Member and the Týnec Formation (Westphalian D – Barruelian) in the Kladno-Rakovník and Pilsen basins. *Bulletin of Geosciences 80(1)*, 45–66.

OPLUŠTIL, S. & PEŠEK, J. 1998. Stratigraphy, palaeoclimatology and palaeogeography of the Late Paleozoic continental deposits in the Czech Republic, 597–620. *In* CRASQUIN-SOLEAU, S., IZART, A., VASLET, D. & DE WEVER, P. (eds) *Peri-Tethys: Stratigraphic Correlations 2. Geodiversitas 20(4).*

OPLUŠTIL, S., SCHMITZ, M., CLEAL, C.J. & MARTÍNEK, K. 2016. A review of the Middle–Late Pennsylvanian west European regional substages and floral biozones, and their correlation to the Geological Time Scale based on new U-Pb ages. *Earth-Science Reviews 154*, 301–335. DOI 10.1016/j.earscirev.2016.01.004

PAŠEK, J. & URBAN, M. 1990. The tectonic evolution of the Plzeň Basin (Upper Carboniferous, Western Bohemia): a review and reinterpretation. *Folia Musei rerum naturalium Bohemiae occidentalis, Geologica 32*, 3–56.

PEIZHEN, Z., MOLNAR, P. & DOWNS, W.R. 2001. Increased sedimentation rates and grain sizes 2±4 Myr ago due to the influence of climate change on erosion rates. *Nature 410*, 891–897. DOI 10.1038/35073504

PEŠEK, J. 1968. Geologická stavba a vývoj sedimentů plzeňské černouhelné pánve. *Sborník Příroda 2*. Pilsen. [in Czech]

PEŠEK, J. 1994. *Carboniferous of Central and Western Bohemia (Czech Republic)*. 60 pp. Czech Geological Survey, Prague.

PEŠEK, J., HOLUB, V., MALÝ, L., MARTÍNEK, K., PROUZA, V., SPUDIL, J. & TÁSLER, R. 2001. *Geologie a ložiska svrchnopaleozoických limnických pánví ČR*. 243 pp. Czech Geological Survey, Prague.

PEŠEK, J., OPLUŠTIL, S., KUMPERA, O., HOLUB, V., SKOČEK, V., DVOŘÁK, J., PROUZA, V. & TÁSLER, R. 1998. *Paleogeographic Atlas: Late Paleozoic and Triassic Formations, Czech Republic*. 53 pp. Czech Geological Survey, Prague.

POTTS, P.J. 1995. *A Handbook of Silicate Rock Analysis*. 622 pp. Blackie Academic and Professional, London. DOI 10.1007/978-1-4615-3270-5

RAMOS, A. & SOPENA, A. 1983. Gravel bars in low-sinuosity streams (Permian and Triassic, central Spain), 301–312. *In* COLLINSON, J.D. & LEWIN, J. (eds) *Modern and ancient fluvial systems. International Association of Sedimentologists, Special Publication 6.*

REYNOLDS, R.C. JR. 1985. *NEWMOD©, a computer program for the calculation of one dimensional diffraction patterns of mixed-layered clays*. R.C. Reynolds, Jr., 8 Brook Road, Hanover, New Hampshire 03755, USA.

ROBINSON, D. & WRIGHT, V.P. 1987. Ordered illite-smectite and kaolinite-smectite: pedogenic minerals in a Lower Carboniferous paleosol sequence, South Wales. *Clay Minerals 22*, 109–118. DOI 10.1180/claymin.1987.022.1.09

ROSENAU, N.A., TABOR, N.J., ELRICK, S.D. & NELSON, W.J. 2013. Polygenetic history of paleosols in middle–upper Pennsylvanian cyclothems of the Illinois Basin, U.S.A.: Part I. Characterization of paleosol types and interpretation of pedogenic processes. *Journal of Sedimentary Research 83(8)*, 606–636. DOI 10.2110/jsr.2013.50

RYGEL, M.C., FIELDING, C.R., FRANK, T.D. & BIRGENHEIER, L.P. 2008. The magnitude of late Paleozoic glacioeustatic fluctuations: a synthesis. *Journal of Sedimentary Research 78*, 500–511. DOI 10.2110/jsr.2008.058

SCHNEIDER, J.W., KORNER, F., ROSCHER, M. & KRONER, U. 2006. Permian climate development in the northern peri-Tethys area – The Lodeve Basin, French Massif Central, compared in a European and global context. *Palaeogeography, Palaeoclimatology, Palaeoecology 240*, 161–183. DOI 10.1016/j.palaeo.2006.03.057

SCOTESE, C.R. & MCKERROW, W.S. 1990. Revised world maps and introduction, 1–21. *In* MC KERROW, W.S. & SCOTESE, C.R. (eds) *Paleozoic Paleogeography and Biogeography. Geological Society of London Memoir 12.*

SHANLEY, K.W. & MCCABE, P.J. 1994. Perspectives on the sequence stratigraphy of continental strata. *American Association of Petroleum Geologists Bulletin 78*, 544–568.

ŠETLÍK, J. 1968. *Fytopaleontologie nýřanských vrstev (zpracování vrtného materiálu) – dílčí závěrečná zpráva*. Ústřední ústav geologický, Prague. [unpublished report]

ŠETLÍK, J. 1977. Results on recent investigations on the Carboniferous flora of Bohemia, 315–340. *In* HOLUB, V.M. & WAGNER, R.H. (eds) *Symposium on Carboniferous Stratigraphy*. Ústřední ústav geologický, Prague.

ŠETLÍK, J. 1980. Makrofytopaleontologie. *In* MALÁN, O. *et al.* (eds) *Plzeňská pánev – černé uhlí – studie*. Ústřední ústav geologický, Prague. [unpublished report]

SHELDON, N.D., RETALLACK, G.J. & TABOR, N.J. 2002. Geochemical climofunctions from North America soils and application to paleosols across the Eocene-Oligocene boundary in Oregon. *Journal of Geology 110*, 687–696. DOI 10.1086/342865

SHELDON, N.D. & TABOR, N.J. 2009. Quantitative paleoenvironmental and paleoclimatic reconstruction using paleosols. *Earth-Science Reviews 95(1–2)*, 1–52. DOI 10.1016/j.earscirev.2009.03.004

SKOČEK, V. 1968. Svrchnokarbonské varvity ve středočeských kamenouhelných pánvích. *Věstník Ústředního ústavu geologického 43*, 113–121. [in Czech with English abstract]

SKOČEK, V. 1970. Silicified wood in the Central Bohemian Permo-Carboniferous. *Věstník Ústředního ústavu geologického 45*, 87–94. [in Czech with English abstract]

SKOČEK, V. 1990. Stephanian lacustrine-deltaic sequence in central and northeast Bohemia. *Sborník geologických věd, Geologie 45*, 91–122. [in Czech with English abstract]

SIEGENTHALER, C. & HUGGENBERGER, P. 1993. Pleistocene Rhine gravel: deposits of a braided river system with dominant pool preservation, 147–162. *In* BEST, J.L. & BRISTOW, C.S. (eds)

Braided rivers. Special Publication 75, Geological Society Publishing House, Bath.

TABOR, N.J. & POULSEN, C.J. 2008. Palaeoclimate across the Late Pennsylvanian–Early Permian tropical palaeolatitudes: A review of climate indicators, their distribution, and relation to palaeophysiographic climate factors. *Palaeogeography, Palaeoclimatology, Palaeoecology 268*, 293–310. DOI 10.1016/j.palaeo.2008.03.052

TANNER, C.B. & JACKSON, M.L. 1948. Nomographs of sedimentation times for soil particles under gravity or centrifugal acceleration. *Soil Science Society of America Proceedings 12*, 60–65. DOI 10.2136/sssaj1948.036159950012000C0014x

ULLAH, M.S., BHATTACHARYA, J.P. & DUPRE, W.R. 2015. Confluence scours versus incised valleys: examples from the Cretaceous Ferron Notom Delta, southeastern Utah, U.S.A. *Journal of Sedimetary Research 85(5)*, 445–458. DOI 10.2110/jsr.2015.34

WATTS, W.L. 1980. Quaternary pedogenic calcretes from Kalahari (southern Africa): mineralogy, genesis and diagenesis. *Sedimentology 27*, 661–686. DOI 10.1111/j.1365-3091.1980.tb01654.x

WEIBEL, R. 1996. Petrified wood from an unconsolidated sediment, Voervadsbro, Denmark. *Sedimentary Geology 101*, 31–41. DOI 10.1016/0037-0738(95)00013-5

WEITHOFER, K.A. 1896. Die geologischen Verhältnisse des Bazer-Schachtes und benachbarten teiles der Pilsner Kohlenmulde. *Österreichische Zeitschrift für Berg- und Hüttenwesen 44(25–28)*, 317–321, 331–335, 345–349, 355–357.

WILDING, L.P. & TESSIER, D. 1988. Genesis of Vertisols: shrink-swell phenomena, 55–81. *In* WILDING, L.P. & PUENTES, R. (eds) *Vertisols: their distribution, properties, classification and management.* Texas A&M University Publishing Center, College Station, Texas.

WILLIS, B.J. 1993. Ancient river systems in the Himalayan fordeep, Chinji village area, northern Pakistan. *Sedimentary Geology 88*, 1–76. DOI 10.1016/0037-0738(93)90151-T

WILSON, M.J. 1999. The origin and formation of clay minerals in soils: past, present and future perspectives. *Clay Minerals 34*, 7–25. DOI 10.1180/000985599545957

WRIGHT, V.P. & MARRIOTT, S.B. 1993. The sequence stratigraphy of fluvial depositional systems: the role of floodplain sediment storage. *Sedimentary Geology 86*, 203–210. DOI 10.1016/0037-0738(93)90022-W

YAALON, D.H. & KALMAR, D. 1978. Dynamics of cracking and swelling clay soils: displacement of skeletal grains, optimum depth of slickensides, and rate of intrapedonic turbation. *Earth Surface Processes and Landforms 3*, 31–42. DOI 10.1002/esp.3290030104

YAGISHITA, K. 1997. Paleocurrent and fabric analyses of fluvial conglomerates of the Paleogene Noda Group, northeast Japan. *Sedimentary Geology 109*, 53–71. DOI 10.1016/S0037-0738(96)00058-9

ŽÁČEK, V. & CHÁB, J. 1993. Metamorphism in the Teplá Upland, Bohemian Massif, Czech Republic (Preliminary report). *Věstník Českého geologického ústavu 68(3)*, 33–37.

ZIEGLER, P.A. 1990. *Geological Atlas of Western and Central Europe. Second edition.* 239 pp. Shell Internationale Petroleum Maatschappij B.V., The Hague.